U.S.N.A. --- Trident Scholar project report; no. 309 (2003)

SCALE-MODEL VEHICLE ANALYSIS FOR THE DESIGN OF A STEERING CONTROLLER

by

Midshipman Philip C. Hoblet, Class of 2003
United States Naval Academy
Annapolis, Maryland

_____
(signature)

Certification of Advisers Approval

Associate Professor Richard T. O'Brien, Jr.
Department of Weapons and Systems Engineering

_____
(signature)

_____
(date)

Assistant Professor Jenelle Armstrong Piepmeier
Department of Weapons and Systems Engineering

_____
(signature)

_____
(date)

Acceptance for the Trident Scholar Committee

Professor Joyce E. Shade
Deputy Director of Research & Scholarship

_____
(signature)

_____
(date)

USNA-1531-2

REPORT DOCUMENTATION PAGE

Form Approved OMB No. 0704-0188

1. REPORT DATE (DD-MM-YYYY)	2. REPORT TYPE	3. DATES COVERED (FROM - TO)
02-05-2003		xx-xx-2003 to xx-xx-2003

4. TITLE AND SUBTITLE
Scale-model Vehicle Analysis for the Design of a Steering Controller
Unclassified

5a. CONTRACT NUMBER
5b. GRANT NUMBER
5c. PROGRAM ELEMENT NUMBER

6. AUTHOR(S)

5d. PROJECT NUMBER
5e. TASK NUMBER
5f. WORK UNIT NUMBER

7. PERFORMING ORGANIZATION NAME AND ADDRESS
US Naval Academy
Annapolis, MD21402

8. PERFORMING ORGANIZATION REPORT NUMBER

9. SPONSORING/MONITORING AGENCY NAME AND ADDRESS
,

10. SPONSOR/MONITOR'S ACRONYM(S)
11. SPONSOR/MONITOR'S REPORT NUMBER(S)

12. DISTRIBUTION/AVAILABILITY STATEMENT
APUBLIC RELEASE
,

13. SUPPLEMENTARY NOTES

14. ABSTRACT

This Trident project investigates the design of a driver assistance steering controller. The initial goal of this research was to modify an off-the-shelf radio controlled (RC) car to make it dynamically similar to full-size automobiles. Using ratios of vehicle parameters (known as P groups), the Buckingham-Pi theorem was applied to analyze both the scale vehicle and a variety of full-size vehicles. To establish the standards by which to modify the RC car, the P groups of actual automobiles have been calculated using published data. Before any of the RC car?s P groups could be calculated, different parameters of the RC car needed to be measured. Based on comparisons of corresponding P groups, appropriate modifications have been made to achieve dynamic similitude. A control system was designed to control the lateral and longitudinal position of the RC car. The control system stabilized the vehicle but will require further tuning to achieve accurate tracking. After performing an experiment consisting of a lane change maneuver, the data from the RC car was compared to data from similar experiments using full-size automobiles. Similarity between the results verifies the dynamic similitude of the RC car and the full-size automobiles.

15. SUBJECT TERMS

16. SECURITY CLASSIFICATION OF:			17. LIMITATION OF ABSTRACT	18. NUMBER OF PAGES	19. NAME OF RESPONSIBLE PERSON
a. REPORT	b. ABSTRACT	c. THIS PAGE	Same as Report (SAR)	57	Cornell, Elizabeth ecornell@dtic.mil
Unclassified	Unclassified	Unclassified			19b. TELEPHONE NUMBER International Area Code Area Code Telephone Number DSN

REPORT DOCUMENTATION PAGE

Form Approved
OMB No. 074-0188

1. AGENCY USE ONLY (Leave blank)	2. REPORT DATE	3. REPORT TYPE AND DATE COVERED
	2 May 2003	

4. TITLE AND SUBTITLE
Scale-model vehicle analysis for the design of a steering controller

5. FUNDING NUMBERS

6. AUTHOR(S)
Hoblet, Philip C. (Philip Craig), 1981-

7. PERFORMING ORGANIZATION NAME(S) AND ADDRESS(ES)		8. PERFORMING ORGANIZATION REPORT NUMBER

9. SPONSORING/MONITORING AGENCY NAME(S) AND ADDRESS(ES)		10. SPONSORING/MONITORING AGENCY REPORT NUMBER
US Naval Academy Annapolis, MD 21402		**Trident Scholar project report no. 309 (2003)**

11. SUPPLEMENTARY NOTES

12a. DISTRIBUTION/AVAILABILITY STATEMENT	12b. DISTRIBUTION CODE
This document has been approved for public release; its distribution is UNLIMITED.	

13. ABSTRACT: This Trident project investigates the design of a driver assistance steering controller. The initial goal of this research was to modify an off-the-shelf radio controlled (RC) car to make it dynamically similar to full-size automobiles. Using ratios of vehicle parameters (known as Π groups), the Buckingham-Pi theorem was applied to analyze both the scale vehicle and a variety of full-size vehicles. To establish the standards by which to modify the RC car, the Π groups of actual automobiles have been calculated using published data. Before any of the RC car's Π groups could be calculated, different parameters of the RC car needed to be measured. Based on comparisons of corresponding Π groups, appropriate modifications have been made to achieve dynamic similitude. A control system was designed to control the lateral and longitudinal position of the RC car. The control system stabilized the vehicle but will require further tuning to achieve accurate tracking. After performing an experiment consisting of a lane change maneuver, the data from the RC car was compared to data from similar experiments using full-size automobiles. Similarity between the results verifies the dynamic similitude of the RC car and the full-size automobiles.

14. SUBJECT TERMS:	15. NUMBER OF PAGES
Scale-model vehicles, Buckingham-Pi, Vehicle Control, Cornering Stiffness	**55**
	16. PRICE CODE

17. SECURITY CLASSIFICATION OF REPORT	18. SECURITY CLASSIFICATION OF THIS PAGE	19. SECURITY CLASSIFICATION OF ABSTRACT	20. LIMITATION OF ABSTRACT

Abstract:

This Trident project investigates the design of a driver assistance steering controller. The initial goal of this research was to modify an off-the-shelf radio controlled (RC) car to make it dynamically similar to full-size automobiles. Using ratios of vehicle parameters (known as Π groups), the Buckingham-Pi theorem was applied to analyze both the scale vehicle and a variety of full-size vehicles. To establish the standards by which to modify the RC car, the Π groups of actual automobiles have been calculated using published data.

Before any of the RC car's Π groups could be calculated, different parameters of the RC car needed to be measured. Based on comparisons of corresponding Π groups, appropriate modifications have been made to achieve dynamic similitude.

A control system was designed to control the lateral and longitudinal position of the RC car. The control system stabilized the vehicle but will require further tuning to achieve accurate tracking.

After performing an experiment consisting of a lane change maneuver, the data from the RC car was compared to data from similar experiments using full-size automobiles. Similarity between the results verifies the dynamic similitude of the RC car and the full-size automobiles.

Keywords

Scale-model vehicles, Buckingham-Pi, Vehicle Control, Cornering Stiffness

Acknowledgements:

I would like to thank my advisors for putting forth so much of their time and patience to help me through this process. I could not ask for better advisors. For two people with much more happening in their lives, they treated me like I was a priority and gave so much time to help me. I would also like to thank my fiancé for her encouragement and understanding and my family for being so supportive. Finally, I thank God for giving me life and the assurance of salvation in His Son, Jesus Christ.

Table of Contents:

1. Introduction

Automobile accidents injure close to ten million people every year [1]. Fortunately, technology is making cars safer with every new model. Seatbelts, airbags, and other advances in automotive design have lowered the number of fatalities in automobile accidents for years. However, these safety measures are designed for use after an accident. A more effective means for lowering injuries and fatalities in automobiles is to prevent accidents from occurring in the first place.

One method of preventing automobile accidents is to design systems that assist the driver in emergency maneuvers. For example, the anti-lock braking system (ABS), when used correctly, can prevent an automobile from skidding and can lower stopping distances. This system is now standard equipment in many new automobiles. Encouraged by the success of ABS and the promise of better technology, engineers all over the world are working to design the next system that will lower accidents and fatalities [1].

Unfortunately, there are few facilities where full-size testing of such systems can occur. An alternative to expensive and potentially dangerous full-size testing is scale-model testing. An examination of the use of scale-models throughout history demonstrates that they are technologically suitable alternatives to tests with full-size equipment. In one of the most influential inventions of the Twentieth century, Orville and Wilbur Wright performed tests using scale wing designs in a wind tunnel before building the first airplane [2]. During the 1960's, scale models of the lunar rover were tested and used in the design of the vehicles that would drive across the surface of the moon [1]. Undoubtedly, these scale models provided the engineers with data that was used in the production of the actual vehicles. However, the data received from

the scale-model tests was useful because it could be converted into information about the full-size vehicle.

One vehicle maneuver that would greatly benefit from scale-model testing is Emergency Turning and Braking (ETB). This maneuver results in numerous accidents caused by the rolling or spinning of automobiles. For the purposes of this research, the full complement of problems associated with ETB are too complex, so the concentration will be on emergency turning at a constant speed. In an emergency turn at a constant speed, a small amount of roll will be present, but it can be neglected to use a simplified model for the vehicle's lateral dynamics.

2. Previous Research

At the University of Illinois at Champagne-Urbana, a group headed by Professor Andrew Alleyne and his students produced a scale-model vehicle platform consisting of a horse exercise treadmill called the Illinois Roadway Simulator (IRS). A fleet of custom built scale-model vehicles was constructed and tested using the Buckingham-Pi theorem to ensure dynamic similarity between the scale-model vehicles and full-size automobiles. Using this apparatus, they have been successful in showing that the IRS accurately simulates a full-size automobile operating on various road conditions.

Last year, a Trident Scholar, Steven Burns, constructed a smaller, less expensive scale-model vehicle platform at the Naval Academy using off-the-shelf parts (Figure 1). This platform consists of a human treadmill and a vision system connected to a computer controller. The computer uses data from the vision system and onboard sensors to regulate the position of the scale vehicle.

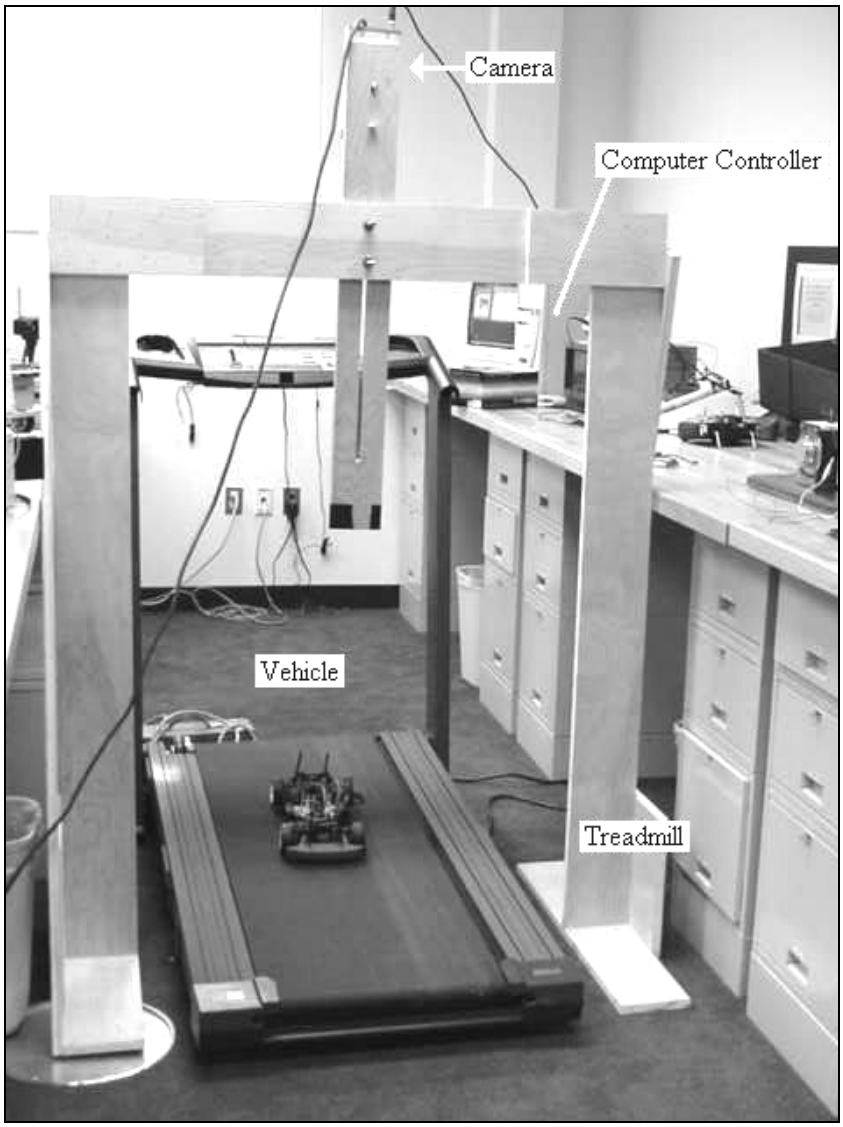

Figure 1: Experimental Apparatus at the U.S. Naval Academy

This year, the platform remains essentially the same. However, the vision system and the software driving it have been upgraded and modified. These modifications enable the control systems to be run in the MATLAB Real-Time environment. The Real-Time environment allows the user to easily implement designs and make modifications to the design while the experiment is running.

3. Background

To make a prediction of the performance of an actual vehicle based on the performance of a scale-model, the two vehicles must be dynamically similar. In other words, the differential equations governing the movements of both systems must be identical after considering the scaling of each parameter in the equations [2].

This requires knowing the equations that govern the vehicle's dynamics and a method for ensuring that the vehicles are dynamically similar. For this, the Buckingham-Pi Theorem is used. For the vehicle dynamics, the Bicycle model and the Dugoff Tire model are used.

3.1 Buckingham-Pi

Dynamic similitude can be shown using the Buckingham-Pi Theorem by replacing the dimensional physical parameters with dimensionless quantities [2]. These ratios are formed using basic units such as length, time, and mass. For example, force could be replaced by [Mass]*[Length]/[Time]^2. Dimensionless groups, known as pi groups are formed from the ratios of physical parameters. The number of pi groups depends on the number of physical parameters and fundamental quantities within a system. If the number of physical parameters in a system is *n*, and the number of fundamental quantities is *m*, then *n-m* Π groups are formed [1]. Each Π group forms a ratio containing information about the system.

According to the theorem, two systems are dynamically similar if the corresponding Π groups are equal [1]. Using this information, one can calculate the requirements for designing a scale-model that is dynamically similar to a full-size vehicle.

3.2 Vehicle Dynamics

To use the Buckingham-Pi theorem, the physical parameters that affect the dynamics of the vehicle must be known. For a complex system like an automobile, the parameters governing the dynamics are so numerous that matching all the Π groups needed to ensure dynamic similitude between the two vehicles would be almost impossible. Due to the emphasis on creating and testing a steering controller for this project, the application of the Buckingham-Pi theorem will be limited to the parameters governing a vehicle's lateral dynamics. One model describing this is the bicycle model.

3.2.1 Bicycle Model

Since the 1950's, engineers have developed different models to describe vehicular motion. One of these models that have been commonly used for controller design purposes is the bicycle model.

The bicycle model simplifies a vehicle's lateral dynamics by assuming that the vehicle is traveling at a constant speed and does not experience pitch or roll. As a result, the equations governing the dynamics of the front tires and rear tires can be mathematically combined to create one front tire and one rear tire, as is the case with a bicycle. By ignoring a vehicle's roll, bounce, and pitch, a vehicle model with three degrees of freedom, yaw and planar motion, can be produced. A complete explanation and derivation of the state equations can be found in [1], and a summary is given as follows.

The state space model for the vehicle's lateral dynamics is:

$$\dot{\underline{x}} = A \cdot \underline{x} + b \cdot u$$

where:

$$\underline{x} = \begin{bmatrix} y \\ \dot{y} \\ \psi \\ \dot{\psi} \end{bmatrix}$$

$$u = \begin{bmatrix} \delta_f \end{bmatrix}$$

$$A = \begin{bmatrix} 0 & 1 & 0 & 0 \\ 0 & -2\dfrac{C_{\alpha f} + C_{\alpha r}}{m \cdot U} & 2\dfrac{C_{\alpha f} + C\alpha_r}{m} & -2\dfrac{a \cdot C_{\alpha f} - b \cdot C_{\alpha r}}{m \cdot U} \\ 0 & 0 & 0 & 1 \\ 0 & -2\dfrac{a \cdot C_{\alpha f} - b \cdot C_{\alpha r}}{I_z \cdot U} & 2\dfrac{a \cdot C_{\alpha f} - b \cdot C_{\alpha r}}{I_z} & -2\dfrac{a^2 \cdot C_{\alpha f} + b^2 \cdot C_{\alpha r}}{I_z \cdot U} \end{bmatrix} \qquad (3.1)$$

$$B = \begin{bmatrix} 0 \\ \dfrac{C_{\alpha f}}{m} \\ 0 \\ \dfrac{C_{\alpha f}}{I_z} \end{bmatrix}$$

The parameters describing the lateral motion of the vehicle are:

$C_{\alpha f}$ ($C_{\alpha r}$)	- Front (rear) Cornering Stiffness
a	- Longitudinal distance from the front axle to the center of gravity
b	- Longitudinal distance from the rear axle to the center of gravity
m	- Mass
U	- Velocity along the longitudinal axis of the automobile
I_z	- Moment of Inertia about the z-axis
d	- Width of wheelbase
r	- Radius of the tire
Ψ	- Yaw angle of the automobile with respect to the inertial frame
δ_f	- The front steering input
y	- The lateral position of the automobile with respect to the inertial frame

Previous research has confirmed that the bicycle model accurately describes the dynamics of actual vehicles in situations where the vehicle experiences less than 0.3 g's [1]. In situations where higher g's are experienced, control systems based on the bicycle model may produce unexpected results.

3.2.2 Dugoff Tire Model

The interaction between the vehicle's tires and the road surface is highly nonlinear. In this work, the Dugoff tire model is used where the force on the tire perpendicular to the wheel plane is assumed to be proportional to the slip angle (Figure 2). The slip angle, α, is defined as the angle between the velocity vector of the tire and the wheel plane.

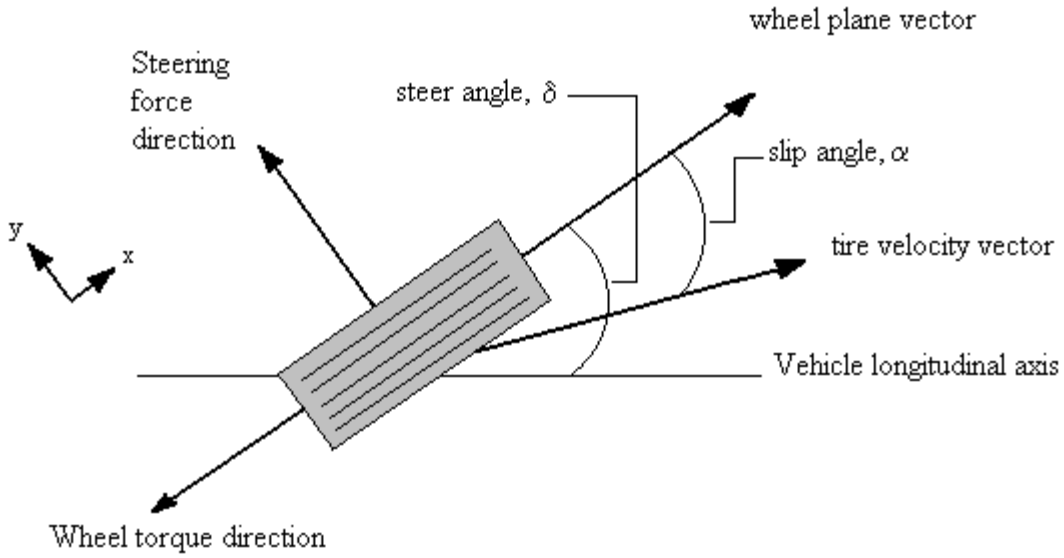

Figure 2: Definition of Tire Slip Angle [1]

The cornering stiffness, C_α, is a constant describing the relationship between the wheel steering force and the wheel angle. The cornering stiffness is defined as $C_\alpha = \left.\frac{\partial F_y}{\partial \alpha}\right|_{\alpha=0}$ where F_y is the force perpendicular to the wheel plane. This linear approximation is accurate for small angles. The method for measuring cornering stiffness experimentally will be described in further detail in a later section.

3.3 Application of Buckingham-Pi Theorem

According to the Buckingham-Pi Theorem, *n-m* Π groups are necessary to ensure two systems are dynamically similar.

From [1], the five Π groups for a vehicle are:

$$\Pi_1 = \frac{a}{L}$$
$$\Pi_2 = \frac{b}{L}$$
$$\Pi_3 = \frac{C_{\alpha_f} L}{mU^2} \quad (3.2)$$
$$\Pi_4 = \frac{C_{\alpha_r} L}{mU^2}$$
$$\Pi_5 = \frac{I_z}{mL^2}$$

where L is the length between the front and rear axles on the automobile, and all other parameters are previously defined.

Π Groups of Actual Automobiles

Before any modifications can be made to the RC car, it is necessary to know the Π groups of actual automobiles. This was accomplished by taking the parameters of nine different automobiles ranging in manufacturer, class, and year from a National Highway Traffic Safety Administration report [4]. Using this data, the Π groups for each of these automobiles have been calculated and are included in Appendix A.

4. Estimation and Modification of Vehicle Parameters

It was previously stated that to produce a dynamically similar scale vehicle, the Π groups of the scale vehicle and the Π groups of the actual, full-size vehicle must be equal. Based on the

Π groups of this vehicle, measuring and altering certain vehicle parameters is necessary. The procedures for measuring some parameters, such as mass and length, need no explanation. However, below is an explanation of the measurement and modification of the RC car's center of gravity and moment of inertia.

4.1 Center of Gravity

Two methods were used to measure the center of gravity. The first method involved balancing the RC car on a thin edge. The second method involved placing the RC car on two scales with the front wheels on one scale and the rear wheels on another scale.

Using the first method, the RC car was balanced longitudinally on a small edge of acrylic as shown in Figure 1. While balanced, the edge was traced on the bottom of the car to show where the car balanced. Then, the car was balanced laterally, and a line is traced to show the edge. The center of gravity was at the point where these two lines intersected.

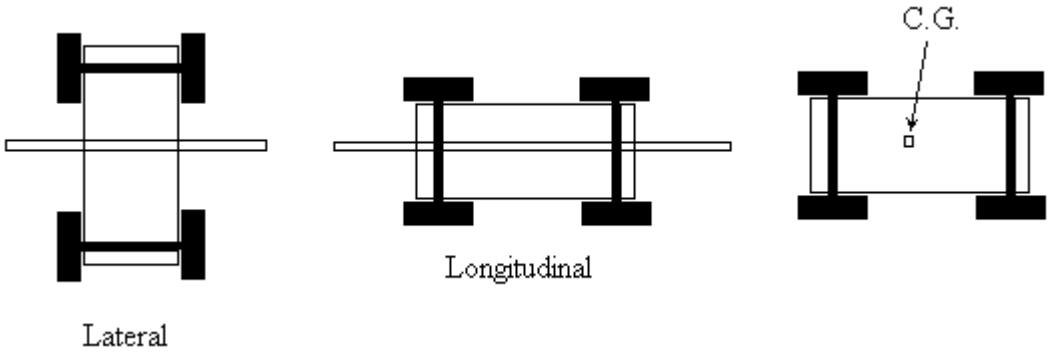

Figure 1: Measuring Center of Gravity

After calculating the first two Π groups, $\prod_1 = \frac{a}{L}$ and $\prod_2 = \frac{b}{L}$, the RC car was compared to a 1989 Ford Escort (Table 1), for example. Looking at the two Π groups, it was clear that the center of gravity on the Ford Escort, as well as most cars, is closer to the front axle than the rear

axle. By thinking about the placement of major components in an automobile, one is able to make sense of this fact. In most automobiles, the engine and transmission are located forward of the lateral centerline. These heavy components move the center of gravity toward the front axle of the automobile. On the RC car, the center of gravity is near the rear axle due to the placement of the motor and battery pack.

Table 1: Comparison of Pi groups

Car	**L**	**a**	**b**	Π_1	Π_2
1989 Escort	2.39 m	0.880 m	1.51 m	0.368	0.632
Unaltered RC car	0.263 m	0.140 m	0.123 m	0.532	0.468

To match the first two Π groups of the RC car with an actual automobile, it was necessary to move the center of gravity of the RC car toward the front axle. Two methods to move the center of gravity exist. The first option adds mass to the front of the RC car in order to offset the weight of the battery pack and the motor. The second method moves existing components on the RC car toward the front axle. Each method makes it possible to match the first two Π groups. However, adding more mass to the RC car changes at least one additional Π group and makes the task of matching other Π groups more difficult or even impossible. Due to these possible adverse side effects, the second method was used.

When looking at the possible components of the RC car to move forward, the battery pack was chosen as the best component to move. The battery pack weighs more than any other single component, and therefore the new position of the battery pack has a greater effect on the center of gravity than the movement of any other single component. More importantly, the battery pack was connected to the motor by cables, which could easily be modified to fit the

position of the battery pack. Finally, moving the battery pack forward was reasonable due to the makeup of actual automobiles where the engine is usually above the front axle.

After placing the battery pack in a more forward position, the vehicle's new center of gravity was measured, and the modified Π groups were calculated. These results are shown and compared with actual automobiles in Table 2. The Π groups of the modified RC car are within the range of the Π groups of the actual automobiles shown in the table and are extremely close to the corresponding Π groups of the 1987 Ford Thunderbird and the 1995 Lincoln Mark VII.

Table 2: Parameters of RC Car after altering Center of Gravity

	L	**a**	**b**	Π_1	Π_2
1989 Escort	2.39 m	0.88 m	1.51 m	0.368	0.632
1980 LeSabre	2.95 m	1.30 m	1.64 m	0.443	0.557
1988 Ranger	2.90 m	1.22 m	1.68 m	0.421	0.578
1989 Wrangler	2.38 m	1.11 m	1.27 m	0.465	0.534
RC Car (First Alteration)	0.259 m	0.105 m	0.154 m	0.405	0.595

To verify the location of the center of gravity, the second method to measure the center of gravity was used. The front tires rested on one scale, and the rear wheels rested on the other scale. This method is shown in Figure 2. In this situation, the longitudinal distances from the front and rear axles to the center of gravity can be found using the equations,

$$F_z f = \frac{W * b}{L} \text{ and } F_z r = \frac{W * a}{L}. \qquad (4.1)$$

Using this method, the location of the center of was verified.

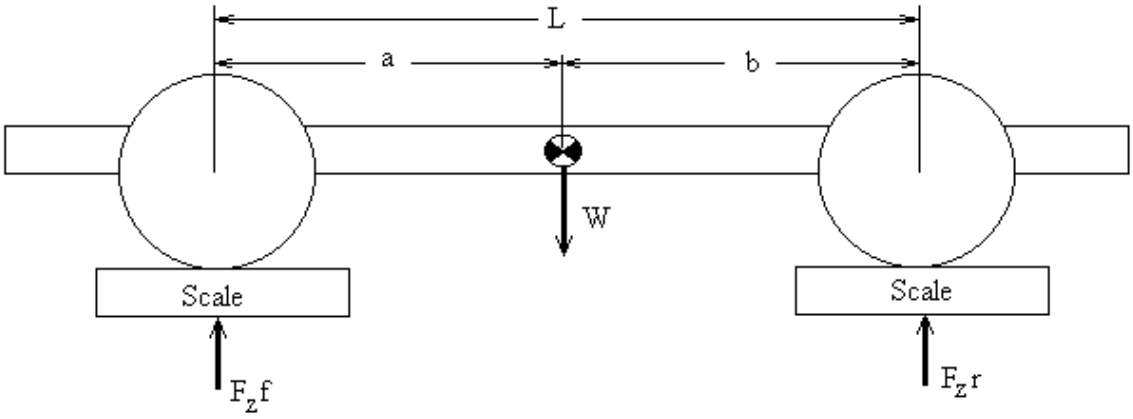

Figure 2: Verifying the Measurement of the Center of Gravity

4.2 Moment of Inertia

The moment of inertia was the second parameter of the RC car requiring modification. This parameter is needed for Π_5, which is $\frac{I_z}{mL^2}$.

The moment of inertia about the z-axis of the RC car, I_z, was found by approximating the RC car's shape and weight distribution by two rectangular blocks as shown in Figure 3. The blocks had the same dimensions and mass as the battery and the rest of the car.

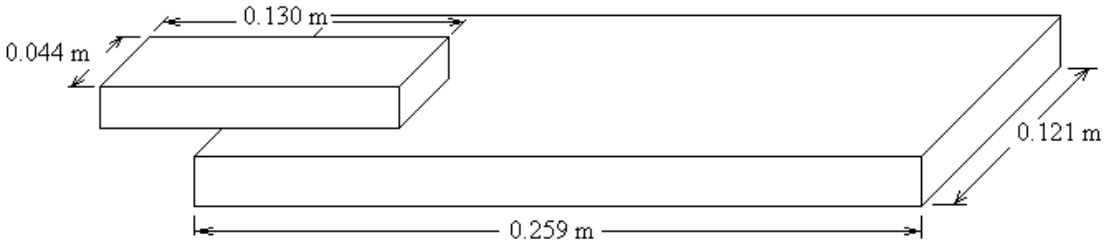

Figure 3: Simplified Shape and Weight Distribution for Estimating I_z

The moment of inertia for each plate is:

$$I = \frac{1}{12} m\left(width^2 + length^2\right) \quad (4.2)$$

For the composite body, the moment of inertia about the z-axis is,

$$I_{total} = I_{car} + m_{car} d_{car}^{\ 2} + I_{battery} + m_{battery} d_{battery}^{\ 2} \quad (4.3)$$

where d_{car} and $d_{battery}$ represent the distance between the center of gravity of each block and the center of gravity of the RC car. Using these equations, I_z and Π_5 was calculated to be 0.0104 kgm^2 and 0.1134, respectively.

Compared to actual automobiles, the Π_5 of the RC car was much smaller as shown in Table 3. Therefore, the RC car needed modification to produce a greater I_z. Since the RC car was previously modified to match the Π groups associated with the center of gravity, the moment of inertia must be increased without changing the vehicle's center of gravity. This was accomplished by adding mass to both the front and rear of the car.

Table 3: I_z and Π_5

Car	Π_5
RC car	0.1134
1989 Ford Escort	0.219
1980 Buick LeSabre	0.257
1989 Jeep Wrangler	0.230
1988 Ford Ranger	0.239

There are two locations on the RC car that were suitable for placing additional mass - the front and rear bumpers (See Figure 4). If these positions were the same distance from the center of gravity, equal mass could be placed on each. However, since the distances were different, the mass added to each bumper must take into account the bumper's distance from the center of gravity to change the moment of inertia without changing the center of gravity. This was accomplished be setting $m_1 d_1 = m_2 d_2$, where m_1 and m_2 are the added masses, and d_1 and d_2 are the respective distances from the center of mass.

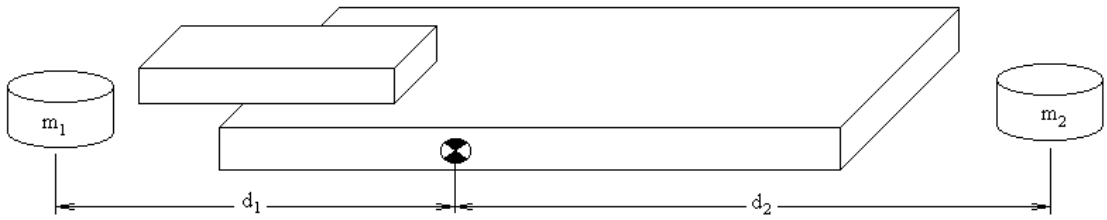

Figure 4: Modified Moment of Inertia

The moment of inertia about the z-axis for a cylinder is: $I_z = \frac{1}{2} m r^2$. Adding two cylindrical masses at a known distance from the center of gravity to the unmodified moment of inertia, gives a total moment of inertia of:

$$I_{modified} = I_{unmodified} + \frac{1}{2} m_1 {r_1}^2 + m_1 {d_1}^2 + \frac{1}{2} m_2 {r_2}^2 + m_2 {d_2}^2 . \qquad (4.4)$$

However, the goal was not to obtain a specific moment of inertia. Instead, the goal was to match the Π_5 of the RC car to the Π_5 of an actual automobile. Using the modified moment of inertia and the new mass, Π_5 was equal to:

$$\Pi_5 = \frac{I_{modified}}{(m + m_1 + m_2)L^2} \tag{4.5}$$

Since the lengths from the center of gravity to the front and rear masses, the radius of the masses, and the relationship between the masses were known, the magnitude of the additional masses was calculated by setting the RC car's Π_5 equal to the Π_5 of an actual automobile. To determine theoretical values for the additional masses, the RC car's Π_5 was set to a value within the range of the Π_5 of the sampled actual automobiles.

For this theoretical exercise, d_1, d_2, and the radii of the masses are 0.155 m, 0.192 m, and 0.03 m respectively.

$$I_{modified} = I_{unmodified} + \frac{1}{2}m_1(0.03)^2 + m_1(0.155)^2 + \frac{1}{2}m_2(0.03)^2 + m_2(0.192)^2 \tag{4.6}$$

Since it was desired for the center of gravity to remain in the same position, m_2 can be written in terms of m_1.

$$m_2 = m_1\left(\frac{0.155}{0.192}\right) = 0.807m_1 \tag{4.7}$$

Using this substitution, m_1 can be determined from the following equation.

$$\Pi_5\ average = \frac{I_{modified}}{(m + m_1 + 0.807m_1)L^2} \tag{4.8}$$

Solving for the additional masses produces values of m_1 = 0.474 kg and m_2 = 0.375 kg.

Because the additional masses varied in diameter and came in incremental masses, calculating the moment of inertia was much more difficult. To aid in calculating different

possibilities for the moment of inertia and its effect on Π_5, a MATLAB script file was created to investigate different combinations and orientations of known masses and radii. The combination of masses implemented on the RC car is shown in Figure 5.

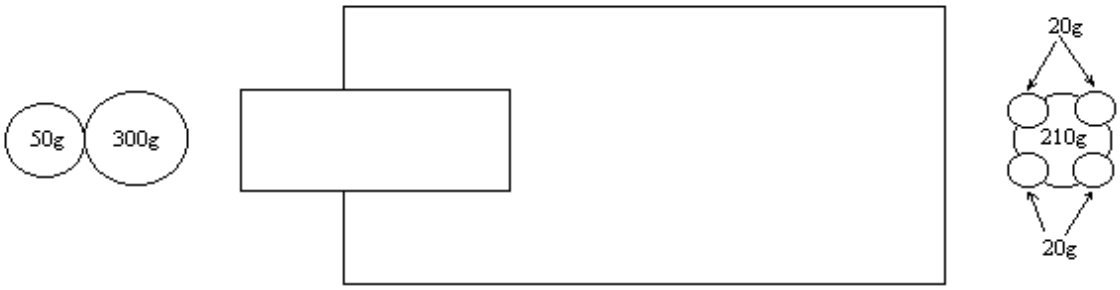

Figure 5: Final Combination of Added Mass

The modified moment of inertia was calculated to be 0.0300 kgm^2. Using the new I_z and the additional mass, a new Π_5 was calculated to be 0.230. This value is closest to the Π_5 of a Jeep Wrangler, but it is also well within the range of the Π_5 of the actual automobiles in this study.

Although great care was taken to ensure that the center of gravity did not change, the center of gravity shifted a small amount. The new center of gravity was measured and results in Π_1 and Π_2 equal to 0.410 and 0.590 respectively.

5. Estimation of Tire Parameters

Along with the vehicle parameters, the tire parameters required investigation to match the Π groups and to produce dynamic similitude between the RC car and actual automobiles. Since the Dugoff Tire Model was used, cornering stiffness, C_α, was the only tire parameter that was needed. Two of the five Π groups depend on cornering stiffness, $\Pi_3 = \frac{C_{\alpha_f} L}{mU^2}$ and $\Pi_4 = \frac{C_{\alpha_r} L}{mU^2}$,

where Π_3 is a function of the front cornering stiffness and Π_4 is a function of the rear cornering stiffness.

5.1 Cornering Stiffness Testing Apparatus

Perhaps the most difficult parameter to measure on the RC car was cornering stiffness. To find the appropriate tires to use on the RC car, five sets of tires, differing in material and traction, were obtained and tested using a special cornering stiffness testing apparatus. This apparatus allows different types of tires to be tested at different speeds.

The cornering stiffness testing apparatus (Figure 6) consists of a movable arm, base, hub and axle assembly, vertical shaft, an optical encoder, added mass, and a weight and pulley set. Since cornering stiffness is a ratio of steering force to slip angle, the two variables that needed to be measured were the slip angle and the steering force. If the movable arm was forced to stay parallel with the direction of the treadmill surface movement, the angle at which the wheel was turned was equal to the slip angle. An optical encoder measures this angle, and a weight set was used to measure the force.

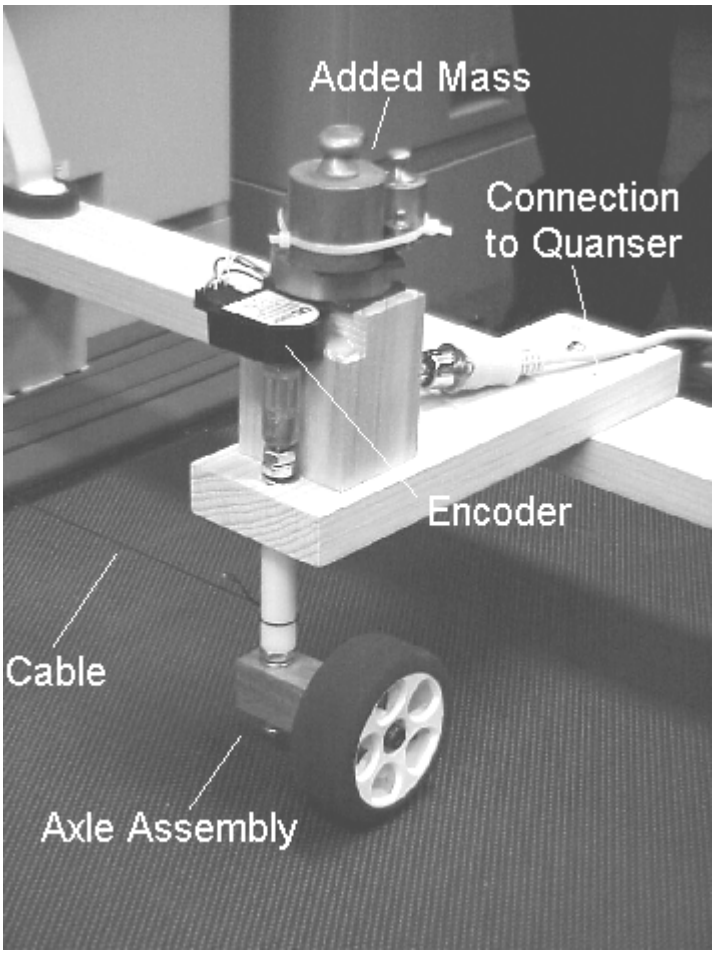

Figure 6: Cornering Stiffness Testing Apparatus

To accurately simulate the conditions under which the tires performed, the axle assembly used the same bearings as the RC car. Also, an amount of mass equal to the loading on the front or rear tires of the RC car was added above the wheel to simulate the loading on the wheel.

The encoder is a US Digital S1 Optical Shaft Encoder. It has 512 counts per revolution. Despite original assumptions that the encoder would need a special circuit to obtain usable data, the encoder was interfaced with existing data acquisition equipment in conjunction with MATLAB's Real-Time Workshop. This discovery not only saved time, but it also allowed the data from the encoder to be read in easily and accurately.

When connected to the data acquisition system, the encoder provided an accuracy of 2048 counts per revolution. This translates to about 0.175 degrees or 0.0031 radians per count. The high level of accuracy provided by the encoder was essential to the computation of cornering stiffness due to the measurements made at small angles.

As was previously stated, the force was supplied by a hanging weight set. This weight set was made up of weights varying from 10g to 300g, dial cord, which has very little elasticity, and a low-friction pulley.

5.2 Procedure for Measuring Cornering Stiffness

The first step in the procedure was to decide whether to test for the cornering stiffness of the front or rear tire. Next, weight was added to the apparatus directly above the wheel for reasons stated previously.

Since the optical encoder is a device that measures relative position, the encoder must be zeroed before the wheel angle can be measured. With the movable arm held parallel to the direction of the treadmill, the position of the axle assembly was adjusted until it was level. Once the axle assembly was level, the wheel angle was zero degrees. The real-time experiment measuring the encoder output was started and the initial wheel angle was 0 degrees. Then, the axle assembly was turned to the desired angle.

As the treadmill was started, the movable arm attempted to turn in the direction of the wheel angle. To keep the movable arm in the correct position, weight was added incrementally to the hanger, which translated to an increase in force perpendicular to the direction of the wheel angle. When this force was great enough to move the wheel in the opposite direction of the wheel angle, the force was recorded.

To obtain the cornering stiffness coefficient for one tire, this procedure was repeated for a number of small angles from 0 to 3.5 degrees. Due to the encoder's characteristics and resolution of 0.175 degrees per count, the wheel angle was increased in increments of 0.35 degrees.

Finally, a linear regression of the force and slip angle data was performed to find the value of the cornering stiffness.

5.3 Experimental Results of Cornering Stiffness Measurement

For this research, five different tires were tested as front tires. These tires varied in manufacturer and material. Three tires were made of a rubber-like material, and two were made of a foam material.

After plotting the data, the data fitting utility in MATLAB was used to find the linear regression of the data. The data for the STS Proline Slick is shown as an example (Figure 7). The cornering stiffness coefficient was equal to the slope of the linear relationship between the steering force and the slip angle. Furthermore, the y-intercept was nearly 0 as expected from the linear model,

$$F_y = C_\alpha \cdot \alpha \qquad (5.1)$$

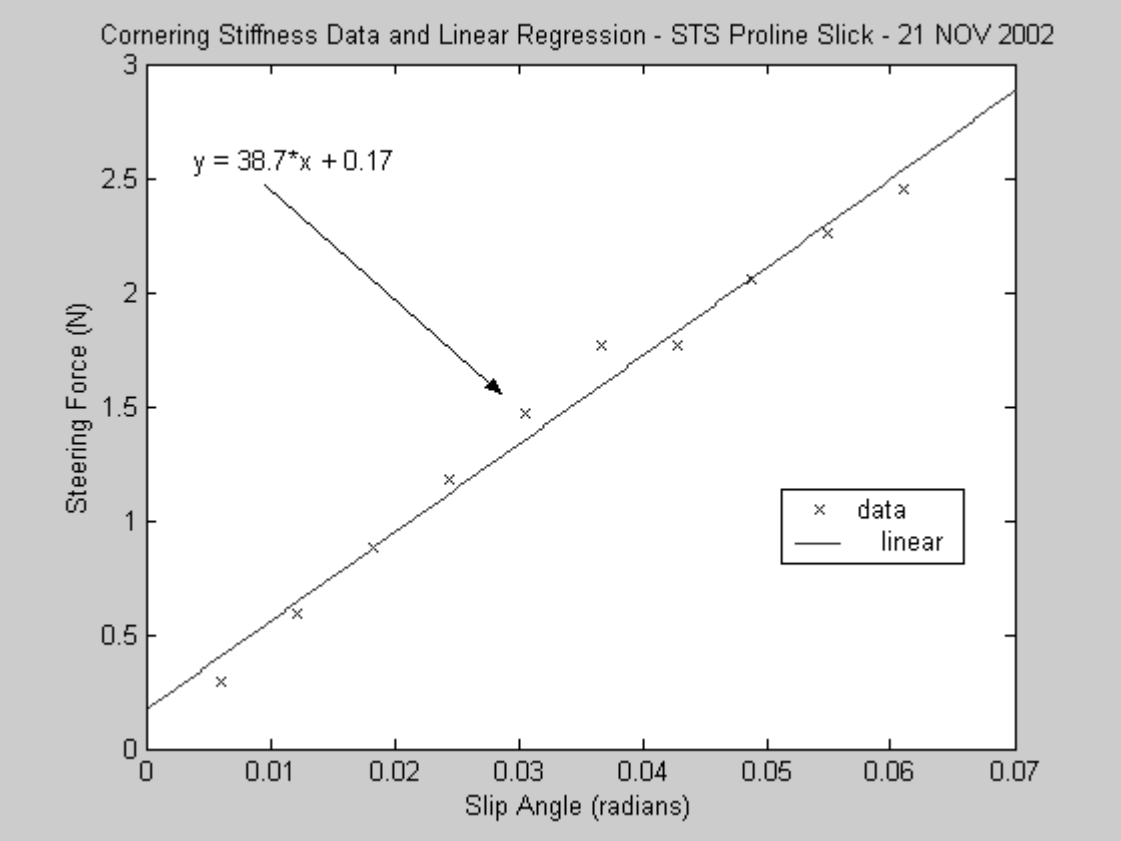

Figure 7: Cornering Stiffness Data

Each of these tires was tested and the data evaluated using the previously described procedure. The cornering stiffness values in Table 4 are the experimental values of cornering stiffness for each of the tires tested. These values were used to determine Π_3 and to approximate the rear cornering stiffness.

Table 4: Cornering Stiffness with 95% Confidence Interval

	Original Tires	**HPI Racing (35R)**	**STS Proline**	**JAC 2164 Pink Sedan**	**JAC 2165 Purple Sedan**
Front Cornering Stiffness, $C_{\alpha f}$	42.7 $\pm$ 5.2 N/rad	50.4 $\pm$ 4.7 N/rad	38.7 $\pm$ 3.5 N/rad	30.2 $\pm$ 2.5 N/rad	25.8 $\pm$ 2.3 N/rad

5.4 Approximation of Rear Cornering Stiffness

Instead of testing each tire with the load correlating to the rear position, a ratio of the rear loading to the front loading was formed. For the modified RC car, this ratio is 0.694. Since, the physical characteristics of the tire did not change with position, multiplying the front cornering stiffness coefficient by the ratio can approximate the cornering stiffness of the tire in the rear position.

To verify that this method of approximating the rear cornering stiffness is valid, one tire (Pink Sedan JAC 2164) was tested with both the front loading and the rear loading. With the front loading, this tire has a cornering stiffness of 30.2 N/rad. With the rear loading, the cornering stiffness is reduced to 22.9 N/rad. Using the ratio to approximate the rear cornering stiffness, a value of 21.0 N/rad is calculated. Because these values are relatively close, the rear cornering stiffness values for the other tires has been calculated using the ratio.

5.5 Buckingham-Pi Analysis of Cornering Stiffness Data

Before calculating the two Π groups associated with cornering stiffness, the Π groups for the actual automobiles needed calculation, and the longitudinal velocity at which the RC car was tested needed measurement.

At a constant velocity, the longitudinal velocity of the RC car is equal to the velocity of the treadmill in the scale-model vehicle platform. This was measured using an on-board sensor mounted next to the treadmill's spin wheel. To use the sensor, +5V was applied to one of the sensor's leads, and the output of the sensor was observed on an oscilloscope.

The output of the sensor shows a spike in voltage with every rotation of the spin wheel (Figure 8). By measuring the time between voltage spikes and the distance that the

treadmill surface travels with one rotation of the spin wheel, the velocity of the treadmill surface can be calculated. Using this method, the velocity was calculated to be 0.850 m/s.

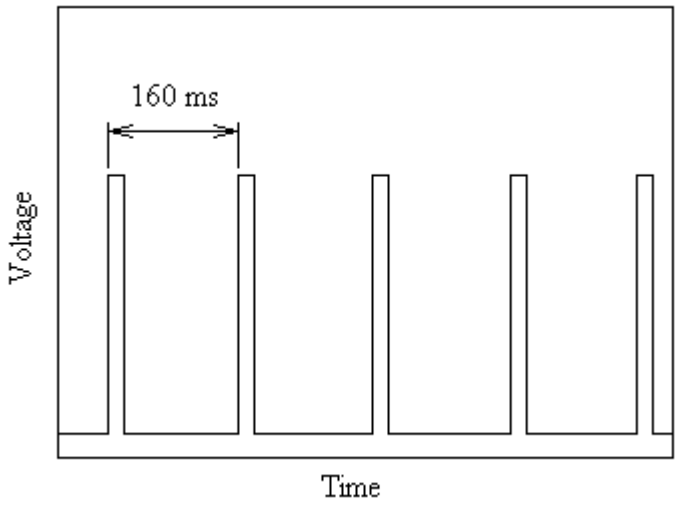

Figure 8: Reproduction of Oscilloscope Picture Showing Sensor Output

In calculating the Π groups for the actual automobiles, an empirical relationship,

$$C_\alpha = (1 - K\mu)\left(\frac{\pi}{4}\right)\left(A_0 + A_1 \cdot F_z - \frac{A_1}{A_2}F_z^2\right) \qquad (5.2)$$

from [3] was used with the coefficients defined in [4].

Using the parameters from the actual automobiles, the front cornering stiffness and Π_3 was calculated for a longitudinal velocity of 60 mph. (Table 5).

Table 5: Cornering Stiffness and Π_3 of actual automobiles at 60 mph

	'89 Escort	**'80 LeSabre**	**'88 Ranger**	**'89 Wrangler**
$C_{\alpha f}$ (lbs/rad)	4956	5932	5335	6470
V (ft/s)	88	88	88	88
Π_3	0.060	0.059	0.071	0.066

In Table 6, the results of calculating Π_3 for a longitudinal velocity are shown. Clearly, the options for Π_3 of the RC car did not equal any of the Π_3 of the actual automobiles. However, this problem could be corrected relatively easily. The velocity of the treadmill could be raised, and the velocity of the actual automobiles could be lowered to make the two Π groups equal. Since the velocity term is squared, the adjustments would not result in unreasonable velocities. Also, there were five tires from which to choose.

Table 6: Initial Π_3 of RC car

	Original Tires	**HPI Racing (35R)**	**STS Proline**	**JAC 2164 Pink Sedan**	**JAC 2165 Purple Sedan**
Π_3	7.23	8.53	6.55	4.37	5.11

Π_3 and Π_4 Matching

To match the groups, Π_3 and Π_4, the appropriate tires for the RC car, the longitudinal velocity of the RC car to travel, and the corresponding velocity of the actual automobiles had to be chosen.

It is conceivable to use any of the sets of tires. However, using the tires with the lowest cornering stiffness coefficient, the JAC 2165 Purple Sedan Tires, was preferable. The lower

cornering stiffness coefficient allows the RC car to travel at a slower velocity while matching the Π groups of the actual automobiles. This decreased speed made the task of control less difficult.

Because emergency turning situations generally occur at higher speeds, it was desired to make the RC car similar to actual automobiles traveling at speeds near 65 mph. To choose the velocity at which the RC car would travel and the velocity that would be used in the Π groups of the actual automobiles, the relationship between the velocity of the RC car and the actual automobiles was determined. For example, to match Π_3 of the RC car and the 1989 Jeep Wrangler, the velocities must be related by the following equation:

$$U_{RC}(m/s) = \sqrt{6.15 * 10^{-3} * U^2_{Jeep}(ft/s)} \qquad (5.3)$$

An Excel spreadsheet was also created that allows the user to adjust each velocity and view the Π groups corresponding to these velocities (Appendix B).

Using the RC car tire with the lowest cornering stiffness, the RC car would have to travel at a velocity near 7.5 m/s to match the Π groups of the actual automobiles. With the current power supply and equipment, the treadmill has a maximum velocity of 1.97 m/s, which produces a Π_3 for the RC car of 0.812. To obtain the Π_3's of the actual automobiles close to this value, the velocity of the actual automobiles must be 17 mph.

It is important to note that the rear cornering stiffness, $C_{\alpha r}$, was determined by multiplying the front cornering stiffness by the ratio of front loading to rear loading of each specific automobile.

Table 7 shows that Π_3 and Π_4 of the RC car, equipped with the JAC 2165 Purple Sedan Tires and traveling at 1.97 m/s was within the range of the Π_3 and Π_4 of the sampled actual automobiles traveling at 17 mph and equipped with standard tires.

Table 7: Ratio of loading and results of Π_3 and Π_4 at 17 mph

Vehicle	Stock RC	**Modified RC**	1989 Ford Escort	1980 Buick LeSabre	1988 Ford Ranger	1989 Jeep Wrangler
Ratio of loading	0.695	**0.695**	0.582	0.795	0.728	0.871
Π_3	1.35	**0.812**	0.745	0.738	0.884	0.825
Π_4	0.938	**0.564**	0.275	0.587	0.644	0.719

Conclusion of Dimensional Analysis

By virtue of the Buckingham-Pi Theorem, the RC car (Figure 9) was dynamically similar to actual automobiles because all five Pi groups were within the range of the corresponding Pi groups of the sampled actual automobiles.

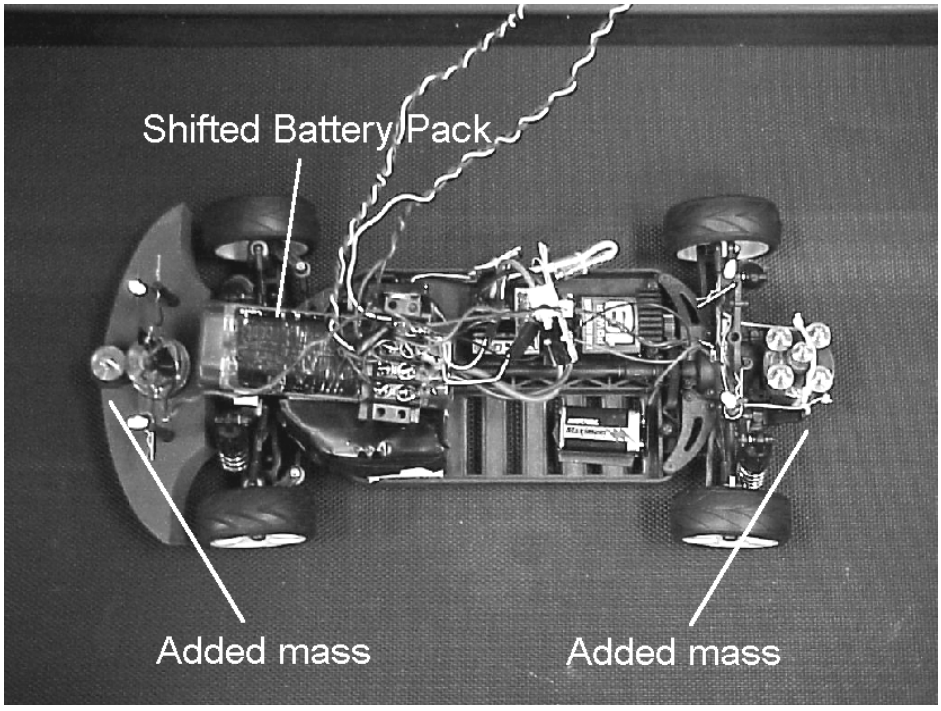

Figure 9: Modified RC Car

6. Vehicle Control

To simulate a human driver's control of an automobile, a system was needed to control the RC car's position. This overall control system was divided into two separate systems. One system was tasked with regulating the RC car's longitudinal position by adjusting the RC car's speed. The other system regulated the vehicle's lateral position by controlling the steering of the RC car.

6.1 Longitudinal Control

Before any control of the RC car's longitudinal velocity could take place, understanding the characteristics of the car's motor and signal processing unit was needed. In order to design the control system for the RC car's longitudinal velocity, it was necessary to keep the RC car's lateral position relatively constant. To accomplish this, the RC car was manually steered using the remote control.

In normal operation, a trigger on a remote control regulates the velocity of the RC car. The signal processing system of the remote converts the amount that the trigger is depressed to an integer between 0 and 255. This integer is then sent to the car's computer. Depending on the value of the integer, the computer sends an analog voltage to the motor, which propels the car. For example, if the trigger on the remote is depressed slightly, the integer, 136, is sent to the car's computer, and the computer sends 1.75 V to the motor.

For this research, the desired velocity of the RC car was slow compared to the velocity at which the RC car was designed to operate. While the voltage supplied to the motor can be more than 7.45 V (integral count = 200), the desired velocity is produced by supplying the car with a voltage closer to 1.75 V (integral count = 136). As the integers increased, the difference in

voltage between integers decreased. As a result, the RC car's speed control has better resolution at higher speeds. The lack of resolution at low speed prevents smooth control of the RC car because the RC car 'jumps' from one speed to another. This non-linearity made the task of keeping the RC car in the center of the test bed track difficult.

Initially, attempts were made to control the car's speed using pulse width modulation. In theory, the integer sent to the RC car's computer would change at such a high frequency that the car would move smoothly and stay in the center of the track. Pulse width modulation did not solve the problem because the RC car's computer could not sample sufficiently fast to make the smooth transitions in speed.

The solution to the problem came in the form of limiting the initial voltage to the car's computer. When fully charged, the battery of RC car provides approximately 8.0 V to power the motor and propel the car. To better control the RC car at slow speeds, the larger integers must correspond to lower voltages. This recalibration was accomplished by reducing the supply voltage (Figure 10). Using this lower voltage, the higher-resolution region corresponds to lower speeds. As a result, there were smoother transitions between speeds. Instead of using the 8.0 V supplied by the car's battery, the car was supplied by 5.33 V from an external power supply. This one-third reduction in the power available to the RC car was large enough to bring the integer counts down to the level at which there were smaller variations in voltage between individual counts, and better, smoother control resulted.

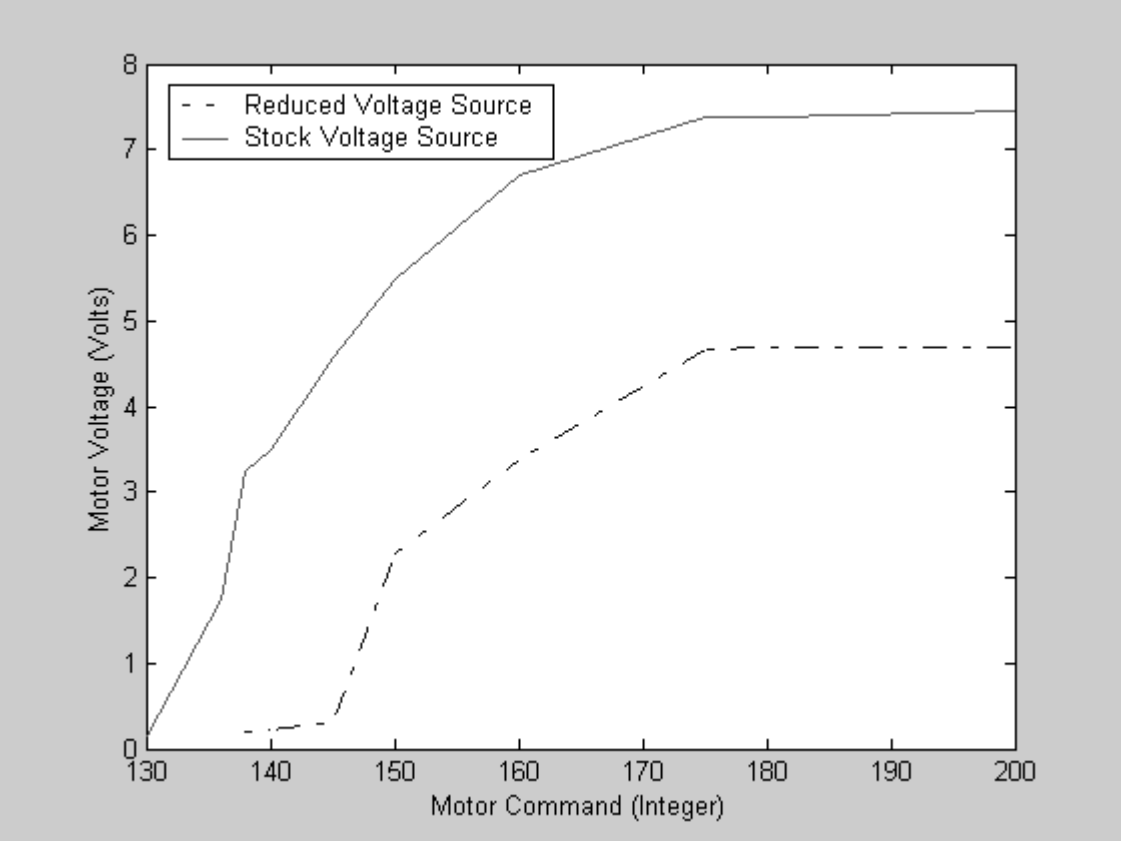

Figure 10: Comparison of Motor Response Due to Stock Voltage Supply and the Reduced Voltage Supply

With the reduced power supplied to the RC car by the external power supply, the RC car's battery pack was not used. However, to preserve the weight distribution necessary for maintaining dynamic similitude with the Pi groups, the battery pack remained in the same position.

With the RC car's voltage supply changed, a closed-loop system was implemented that systematically increased or decreased the count sent to the car's computer depending on the car's longitudinal position with respect to the desired position. The use of the proportional controller resulted in a moderate oscillation of the car's position.

To improve the control system, a Proportional Integral Derivative (PID) compensator was implemented in the closed loop controller (Figure 11). The integrator of the PID compensator

eliminated any steady-state error in the longitudinal position of the RC car. The derivative portion of the PID compensator improved the transient portion of the RC car's response by reducing the oscillation in the position. With the control system enabled, the designed values of the compensator gains were adjusted, and the effect on the performance of the system was experimentally observed. The gains used in the system were chosen because they produced quick and smooth performance. A SIMULINK Diagram of the longitudinal control system can be found in Appendix C.

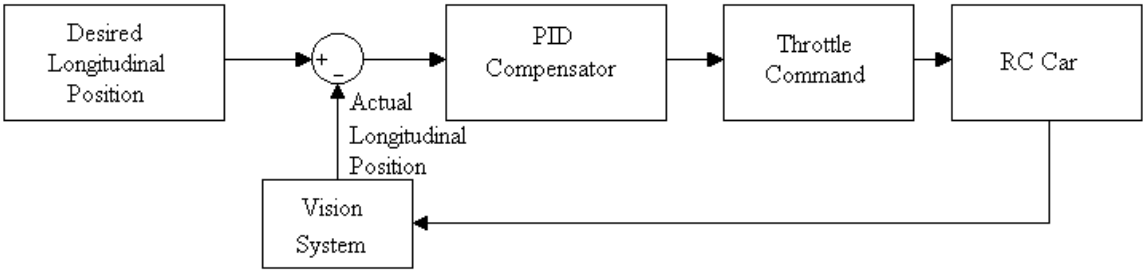

Figure 11: Simplified Block Diagram of the Longitudinal Control System

With this compensator in place, the RC car's longitudinal position stayed relatively constant and responded well to disturbances. In Figure 12, the response of the system is shown when the RC car is given command to go to a new position. While there was some minor oscillation in position when the system responded to a change, these oscillations decreased quickly and smoothly until the position remained within a centimeter of the desired position.

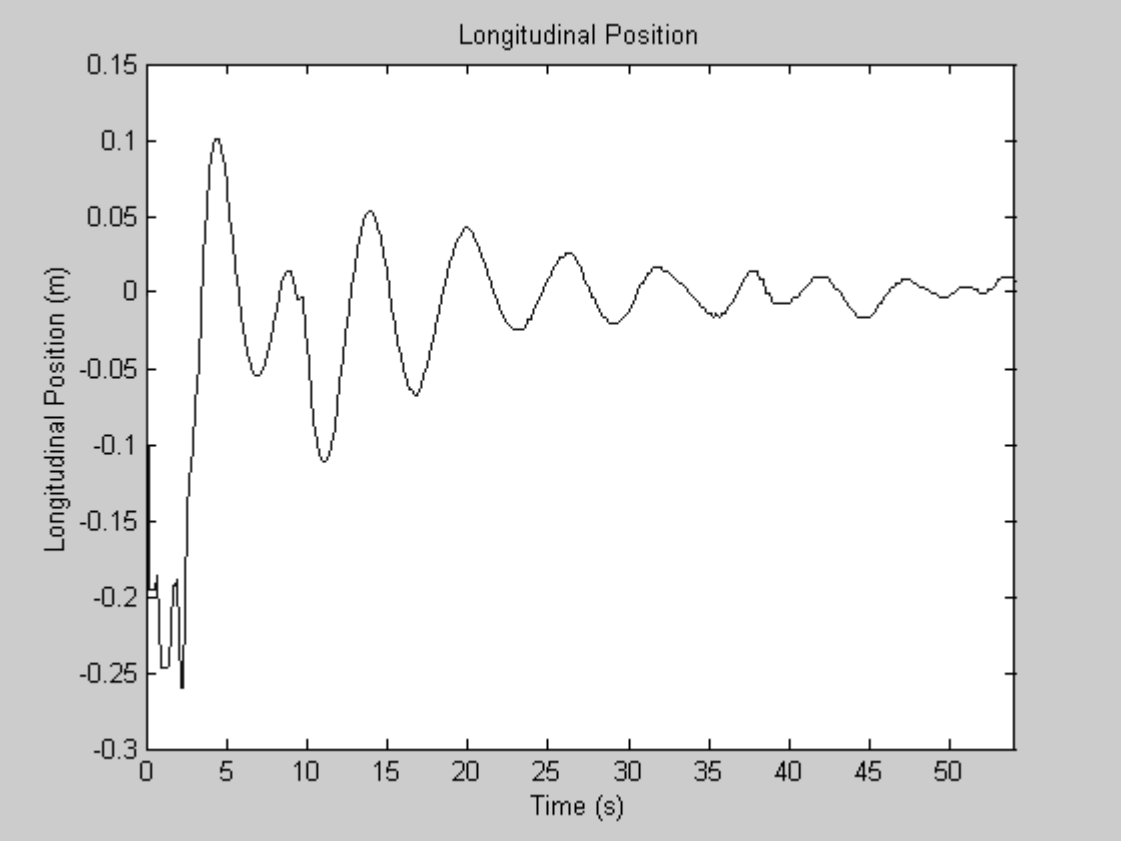

Figure 12: Response RC Car with Longitudinal Control System Enabled

6.2 Lateral Control

Before designing any controller to provide the car with lateral control, the relationship between the wheel angle and the integer given by the computer to the steering servomotor needed to be identified.

This was accomplished by creating a simple experiment in which an integer was given to the servomotor. Then, the angle to which the wheels turn was measured (Figure 13).

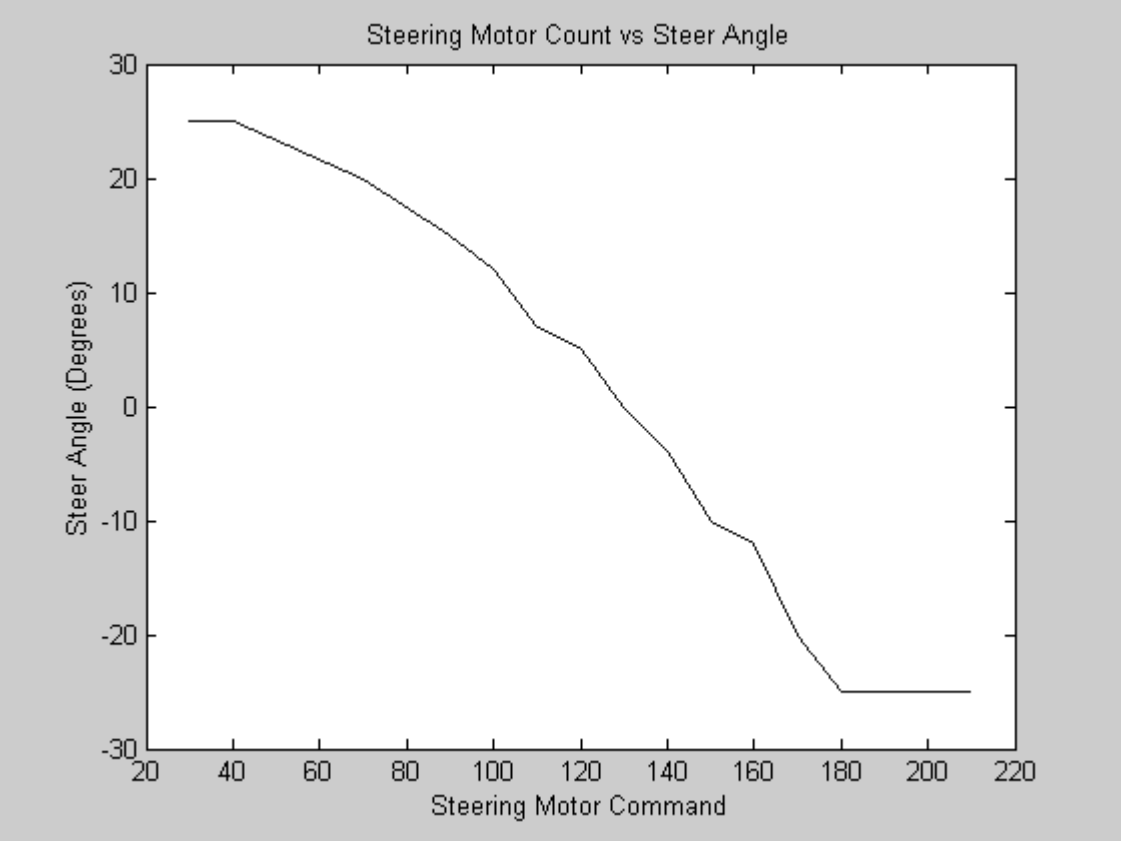

Figure 13: Relationship between the Steering Motor Command vs. Steer Angle

After the data about the integer-wheel angle relationship was determined, a control loop was created to read in the RC car's lateral position and yaw from the camera (Figure 14). The lateral position and yaw were compared to the corresponding desired values, and the errors were combined to create the steering command. Using the measured parameters of the RC car and the bicycle model of lateral dynamics, a SIMULINK model of the lateral control system was used to design and test various compensators. In practice, this was a reasonable method of control, but implementing the lateral control system was a difficult task.

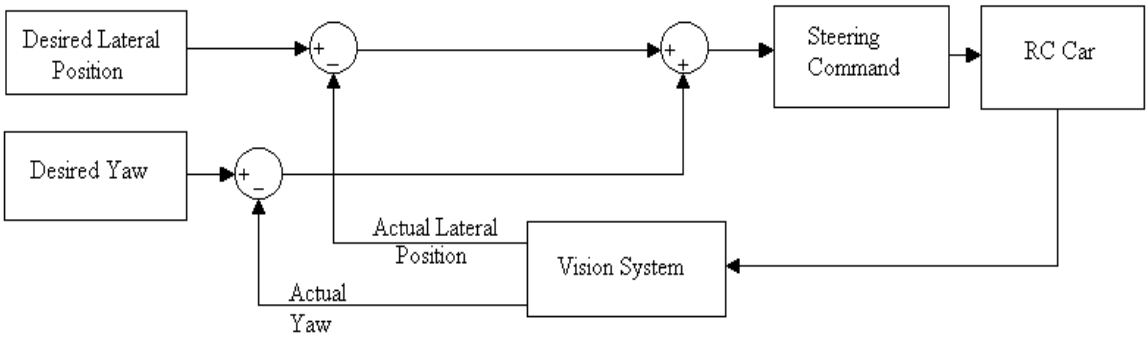

Figure 14: Simplified Block Diagram of Lateral Control Loop

With the RC car and control system modeled, it was hoped that the simulation would accurately represent the experimental apparatus. However, this was not the case. When the initial lateral control system was implemented, the RC car suffered an increasing oscillation until complete instability was observed and the car drives off the track.

With the control system activated, the steering motor behaved erratically. This behavior led to the suspicion that noise was affecting the performance of the system. Simulations including the effects of noise verified this suspicion showing that the presence of noise severely degraded performance.

To accurately remedy the situation, a number of modifications to the simulation were made including the incorporation of sampling delays to examine the effects of the sampling time, analog and digital compensators to reduce the effects of sampling time, and low pass filters to attenuate noise.

Ultimately, a servomotor from a different manufacturer was installed. With the new servomotor, less noise was present in the system, and the control system worked reasonably well. The lateral control system was stable, but the vehicle continued to experience moderate oscillation in lateral position as illustrated in Figure 15. As a result, the control system lacks the ability to make the vehicle move to a desired lateral position and remain at that position until a

new desired position is given. Due to the time spent on troubleshooting, there was insufficient time to further tune the lateral controller. The SIMULINK diagram of the lateral and longitudinal control system can be found in Appendix D.

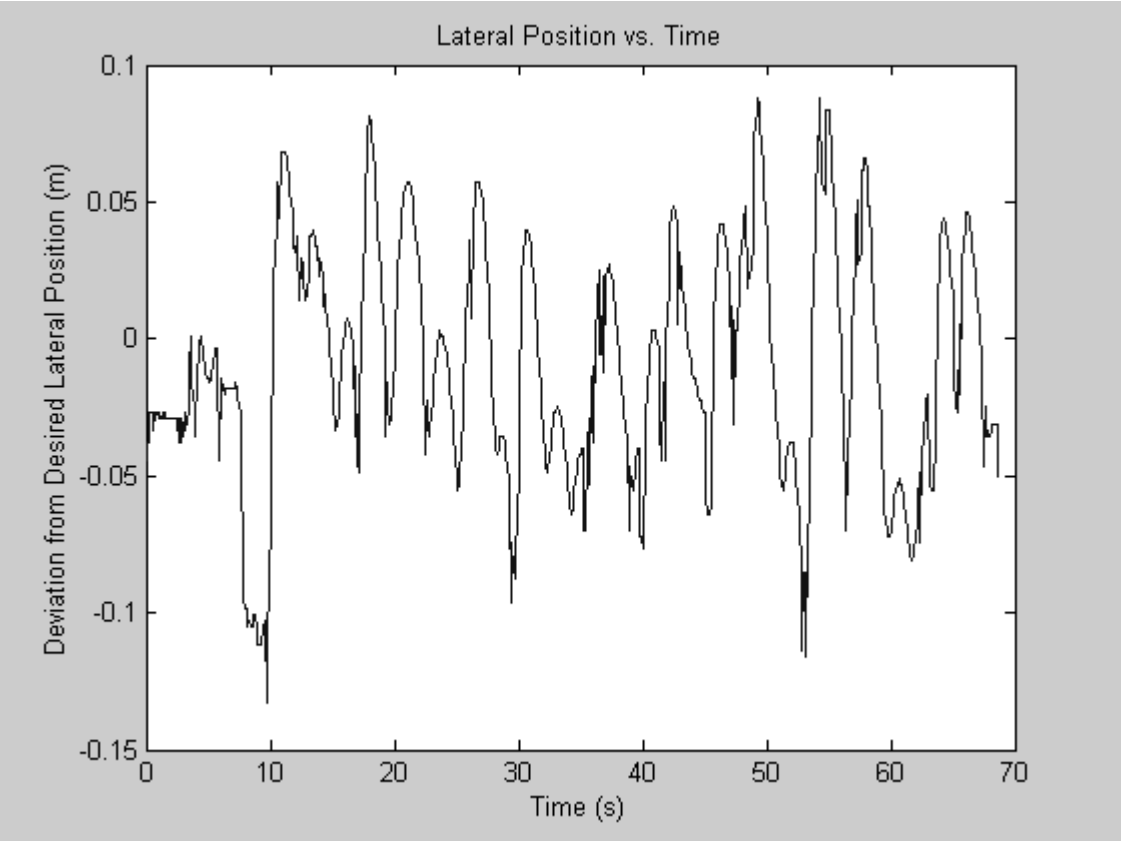

Figure 15: Oscillation in Lateral Position with Lateral Control System Enabled

Since lateral control was necessary for other testing, a decision was made to disable the lateral control system and control the lateral position manually by using the remote control. While this was not a perfect solution, it allowed experimentation to continue.

7. Data Acquisition and Analysis

Two systems were used to acquire data. The longitudinal position, lateral position, and yaw angle of the RC car were measured using the vision system. The DVT Smart Sensor camera

with on-board image processing computed this information and relays the data via an RS232 connection. The second system used to acquire data was composed of two Analog Devices ADXL202 accelerometers and their accompanying software. Some analysis was needed to gain data from these accelerometers about the yaw rate and acceleration of the RC car.

7.1 Accelerometers

Accelerometers were used to obtain data for the lane change maneuver and will be used for the driver assistance steering controller. For the lane change, the data from the accelerometers was used to obtain the RC car's lateral acceleration. In the driver assistance steering controller, the data from the accelerometers will be converted to information about the RC car's yaw rate. If the yaw rate exceeds a certain threshold, the controller will act to augment the driver's input in order to reduce the yaw rate to an acceptable level.

7.1.1 Gaining Data from Accelerometers

The accelerometers used were the Analog Devices ADXL202. This accelerometer measured acceleration in two directions, x and y, but in order to obtain the acceleration data, some analysis was needed. The output of the accelerometers was a four bit string that contained four integers representing the most significant and least significant bits of x and y (X_{MSB}, X_{LSB}, Y_{MSB}, and Y_{LSB}). These were converted into the percentage of Pulse Width Modulation for the current acceleration by the formula:

$$PWM\ \% = (256*MSB + LSB)/100 \qquad (7.1)$$

The PWM% corresponds to the acceleration in g's. For example, 50% equals 1 g or 9.81 m/s^2.

Initially, it was thought that the accelerometers could be introduced into the control loop in SIMULINK through the serial ports. However, with these blocks set, the data was too noisy for the relatively small accelerations that the RC car would experience, and it was not synchronized in time. Attempts were made to overcome the noise by creating and implementing low-pass filters, but no filter appeared to obtain satisfactory results. As for the time delay in the data, several attempts were made to reduce the time delay, but in the end, a delay of approximately one second remained. This delay was much too long for these accelerometers to be used in a control system.

Although the current accelerometers were unsuitable for a control system, they could be used to gain data that to be analyzed after the experiment. Using the software that came with the accelerometers, the data could be logged and analyzed in MATLAB.

7.1.2 Measuring Lateral Acceleration and Yaw rate with Accelerometers

The kinematic equations of a rigid body [5] were used to relate the acceleration of two points, A and B, on a body to the body's angular acceleration, $\bar{\alpha}$, and angular velocity, $\bar{\omega}$, using the following equation:

$$\bar{a}_B = \bar{a}_A + \bar{\alpha} \times \bar{r}_{B/A} + \bar{\omega} \times \left(\bar{\omega} \times \bar{r}_{B/A} \right) \tag{7.2}$$

Assuming there is a negligible amount of pitch and roll, two coplanar accelerometers mounted at locations A and B produce the following relationships:

$$\begin{bmatrix} a_{B_x} - a_{A_x} \\ a_{B_y} - a_{A_y} \end{bmatrix} = \begin{bmatrix} -r_x & -r_y \\ -r_y & r_x \end{bmatrix} \begin{bmatrix} \omega_z^{\,2} \\ \alpha_z \end{bmatrix} \tag{7.3}$$

where ω_z and α_z represent yaw rate and acceleration, respectively, and r_x and r_y represent the components of $\bar{r}_{B/A}$, the distance from point A to B.

To confirm that the accelerometers could be used to measure yaw rate, an experiment was created. In this experiment, two accelerometers were mounted on a small board. The board was attached to a DC servomotor apparatus using the MATLAB real-time environment and regulated to turn at a constant speed. With the motor's angular velocity constant, data was collected from the accelerometers. This data was analyzed and placed in the following equation:

$$\begin{bmatrix} r_x \\ r_y \end{bmatrix} = \begin{bmatrix} -\omega_z{}^2 & -\alpha_y \\ -\alpha_y & \omega_z{}^2 \end{bmatrix}^{-1} \begin{bmatrix} a_{Bx} - a_{Ax} \\ a_{By} - a_{Ay} \end{bmatrix} \tag{7.4}$$

If the accelerometers were accurately collecting data, the calculated values of r_x and r_y should be equal to the manually measured values.

After the experiment was run, the data was analyzed (Figure 16). Although the data was very noisy, the calculated values for r_x and r_y were extremely close to the measured values (Table 8). This verified the assumption that the accelerometers can be used to measure yaw rate and calibrated the values for r_x and r_y.

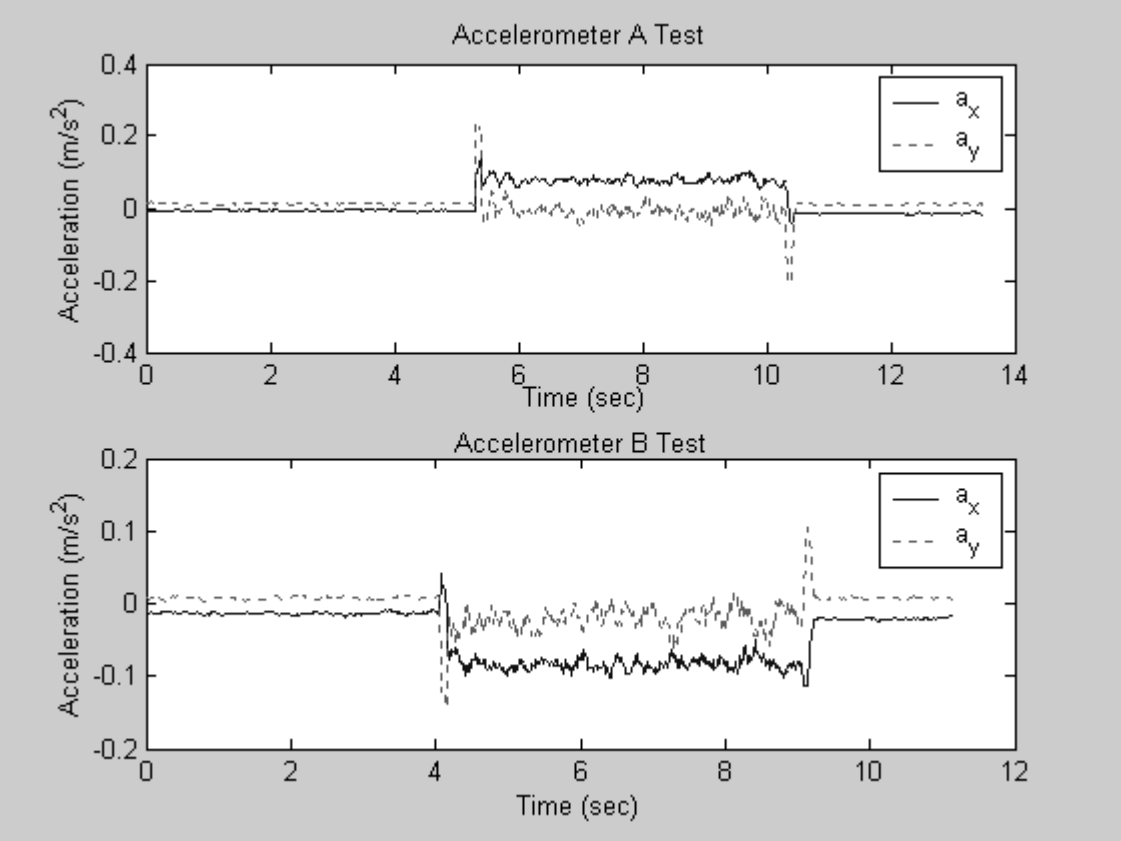

Figure 16: Results of Accelerometer Experiment

Table 8: Comparison of Measured and Calculated Values of r_x and r_y

	r_x	r_y
Measured	0.145 m	0.005 m
Calcuated	0.146 m	0.010 m

While Equation 7.3 could be used to calculate the magnitude of the yaw rate, it could not be used to calculate the sign of the yaw rate. From [5], Equation 7.5 can calculate the sign and magnitude of the yaw rate.

$$\overline{v}_A - \overline{v}_B = \overline{\omega} \times \overline{r}_{B/A} \qquad (7.5)$$

To measure the lateral acceleration of the RC car, the following equation was used,

$$\bar{a}_{CG} = \bar{a}_A - \bar{\alpha} \times \bar{r}_{A/CG} + \bar{\omega} \times (\bar{\omega} \times \bar{r}_{A/CG}) \qquad (7.6)$$

where, $\bar{a}_{CG}$ is a vector describing the acceleration of the center of gravity, $\bar{a}_A$ is a vector describing the acceleration of one of the accelerometers, $\bar{\alpha}$ is a vector describing the angular acceleration of the body (calculated from Equation 7.3), $\bar{r}_{A/CG}$ is a vector describing the position of the accelerometer with respect to the center of gravity, and $\bar{\omega}$ is a vector describing the yaw rate (calculated in Equation 7.5) .

8. Experimental Results

Lane Change Maneuver:

As stated previously, the lane change maneuver was performed to verify that the modified RC car was dynamically similar to full-size automobiles traveling at 17 MPH. Previously, it was planned that the RC car's position would be totally controlled by the control system. However, due to the limited capabilities of the lateral control system, both a computer and a human operator controlled the position of the RC car on the test bed. The computer controlled the longitudinal position of the RC car, and the human controlled the lateral position with a remote control. While a human operator is not able to produce exactly the same movement with each attempt, it is worth noting that the lane change data from the actual automobiles was obtained in tests using human drivers.

The lane change maneuver experiment consisted of the RC car moving from one side of the test-bed track to the other side. During the experiment, the vehicle's longitudinal position, lateral position, and yaw angle was measured by the vision system along with the data from the accelerometers.

With the longitudinal position controlled by the computer and the lateral position controlled manually, the RC car performed the lane change. Although the vision system was not used in the lateral control loop, it was used to record the lateral position of the RC car during the maneuver (Figure 17). This data from the vision system verified that the maneuver was correctly performed. Also, it could be used to verify the results of the data from the accelerometers.

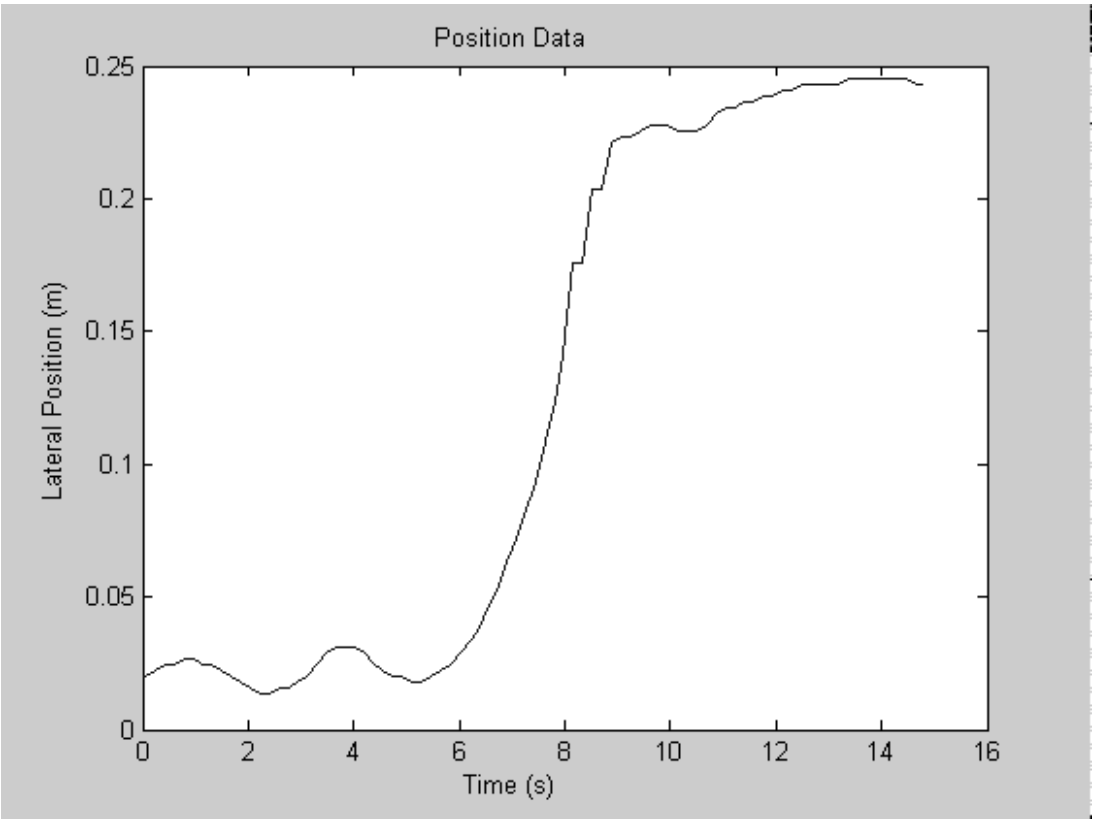

Figure 17: Lateral Position of RC Car during the Lane Change Maneuver

While analyzing the data taken during a test of the RC car's movement on the test bed, the raw data from the accelerometers was extremely noisy (Figure 18). Although accelerometers are known for their noisy data, the periodic nature of the signal suggested that slight vibrations in the suspension of the RC car were affecting the acceleration. The slight irregularities of the surface on the test-bed track could have caused this disturbance. By examining the data, it appeared that these vibrations were periodic and consistently had a period of 0.4 seconds.

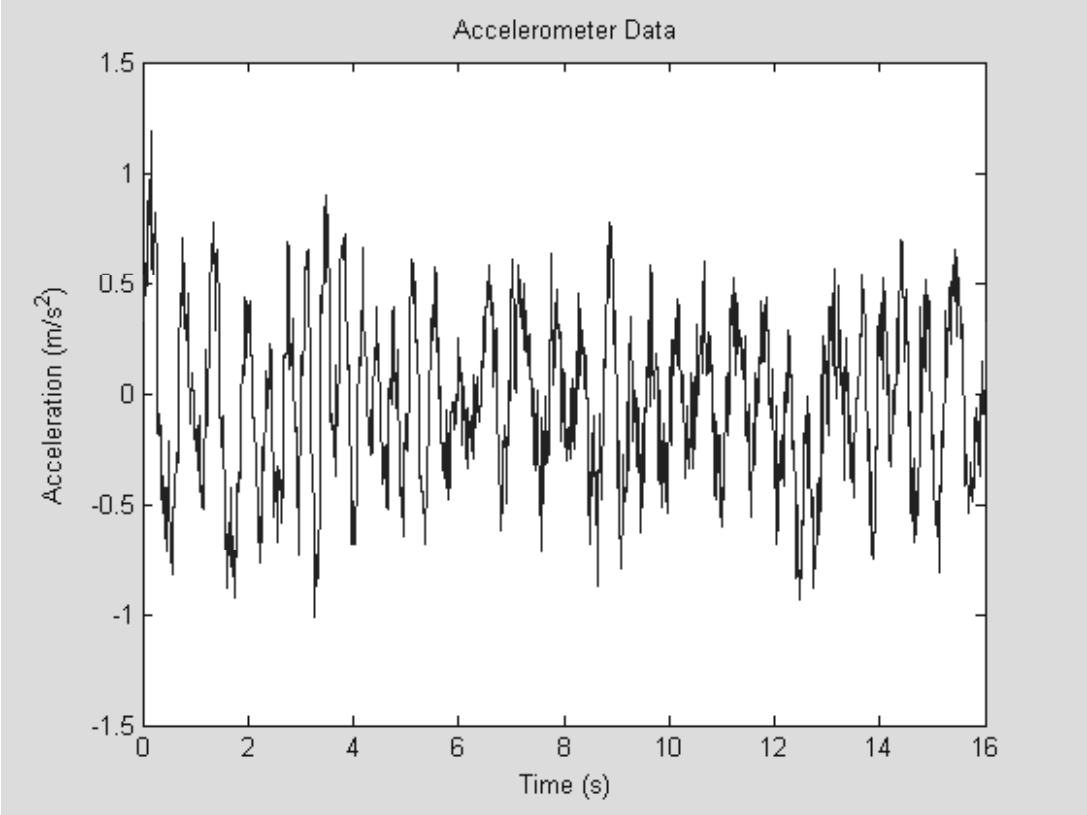

Figure 18: Accelerometer Data from the Lane Change Maneuver

Since the information contained in the frequencies above and below the frequency of the vibration was important, a low-pass filter or high-pass filter was not feasible. However, the notch filter, or stop-band filter, was ideal for this situation. The notch filter reduces the noise in a specific frequency range and does not change the data outside this range. The notch filter has a transfer function of:

$$G(s) = \frac{s^2 + 2\zeta_1 \omega_n s + \omega_n^2}{s^2 + 2\zeta_2 \omega_n s + \omega_n^2} \tag{8.1}$$

where ω_n is the frequency to be filtered out, and ζ_1 and ζ_2 determine the sharpness of the edges of the filter with $\zeta_1 < \zeta_2$.

The Bode plot (Figure 19) shows the effect of the notch filter on the frequency of the oscillation. This filter eliminated most of the noise associated with the oscillation of the RC car. This enabled the lateral acceleration data to be seen more clearly and analyzed more precisely.

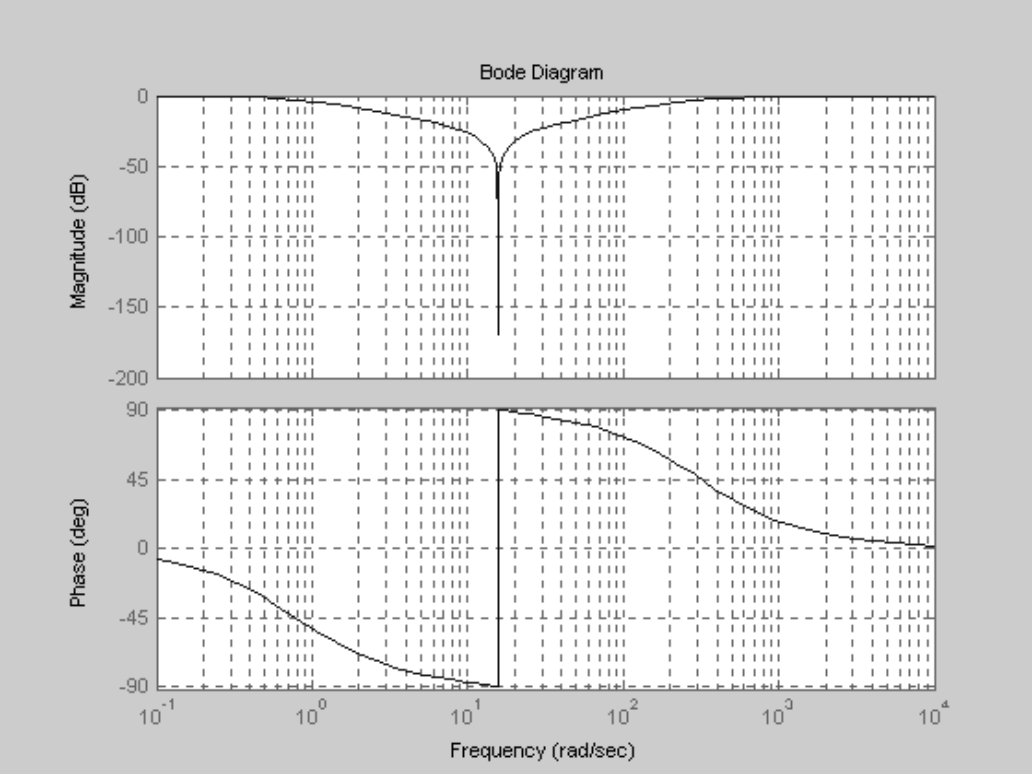

Figure 19: Bode Plot of the Notch Filter

After the accelerometer data was filtered, the true shape of the data was seen more clearly (Figure 20). Then, the filtered data from both accelerometers was integrated, and the yaw rate of the RC car, ω_z, was calculated in accordance with Equation 7.5.

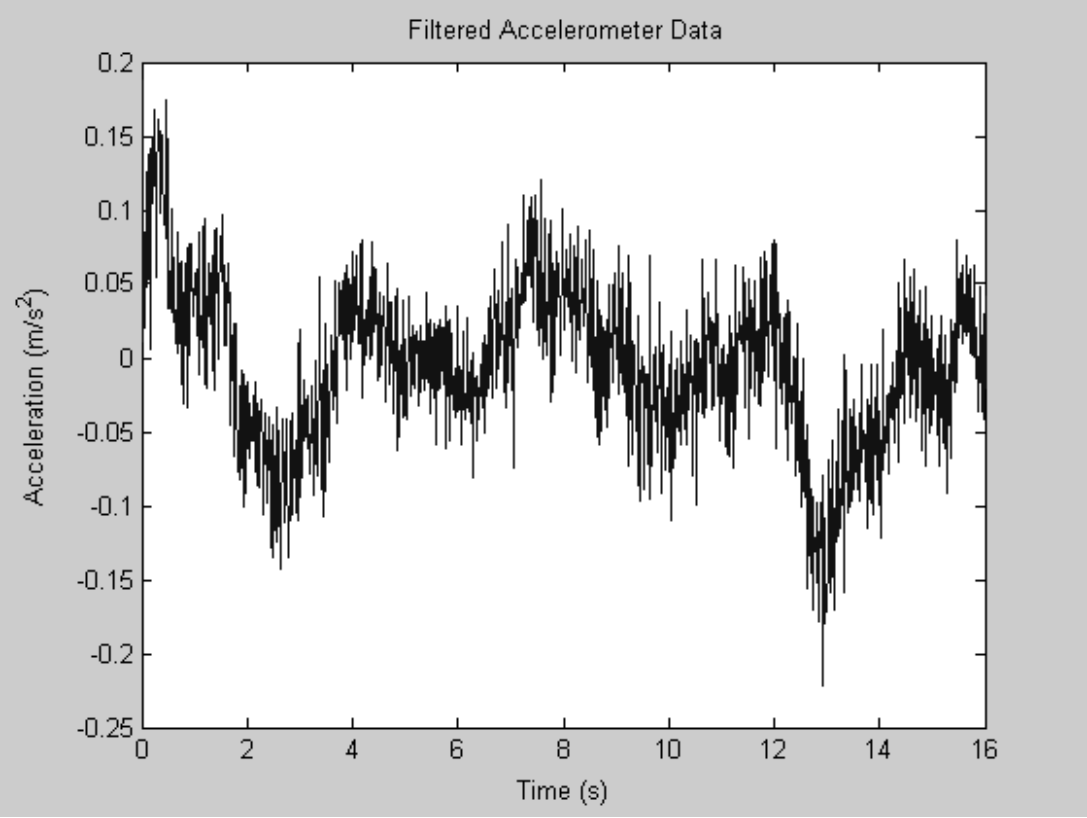

Figure 20: Notch Filtered Data from One Accelerometer in One Direction

After analyzing the yaw rate data, differences materialized between the experimental data and the theoretical lateral acceleration (Figure 21). Theoretically, the yaw rate should look like a sine wave during the lane change. In this set of data, the actual motion of the lane change occurred between 5 seconds and 10 seconds (see back to Figure 17). The yaw rate during this period exhibited a shape like a sine wave, but it was offset. The yaw rate before and after the lane change maneuver should be negligible, since the RC car maintained its yaw angle during this time, but, after looking at the data, it was clear that this was not the case.

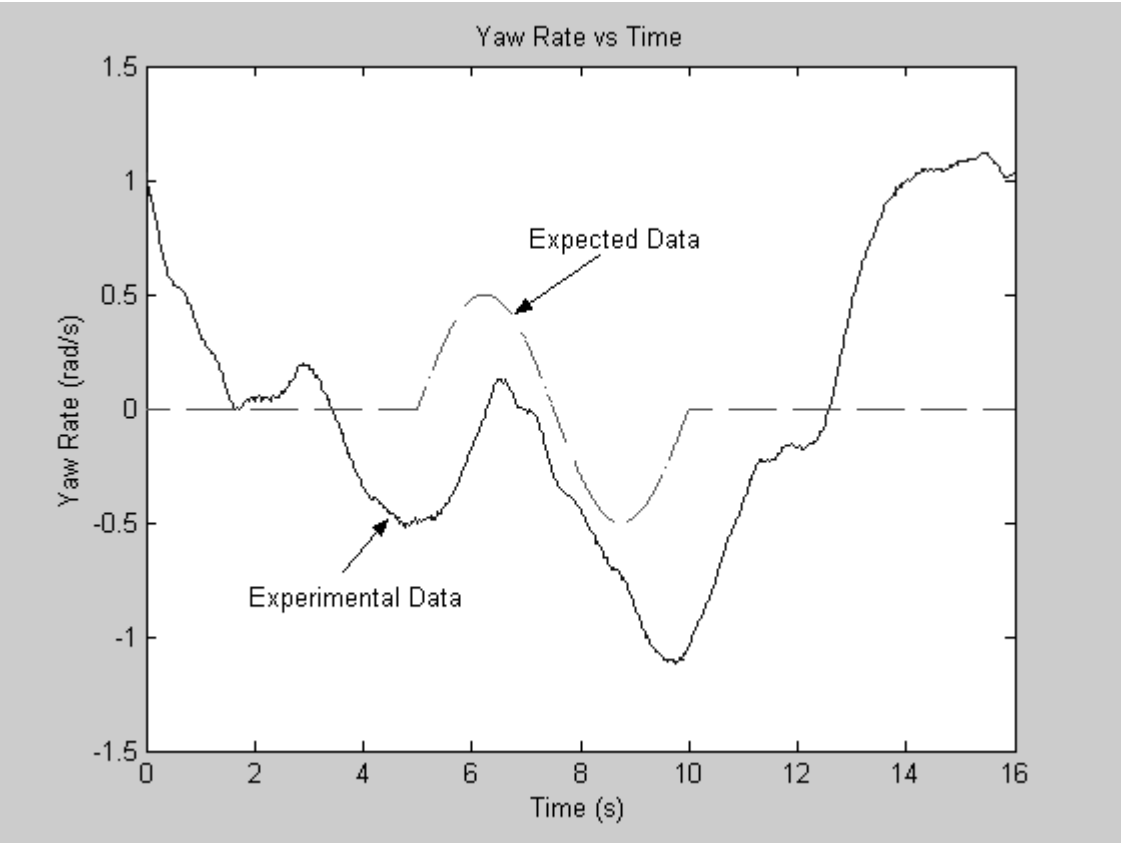

Figure 21: Yaw Rate of RC Car During Lane Change Maneuver

Since the yaw rate was used in the computation of the lateral acceleration (Figure 22), the validity of the lateral acceleration data was questionable. However, the lateral acceleration was consistent with published data from passenger comfort studies [6,7].

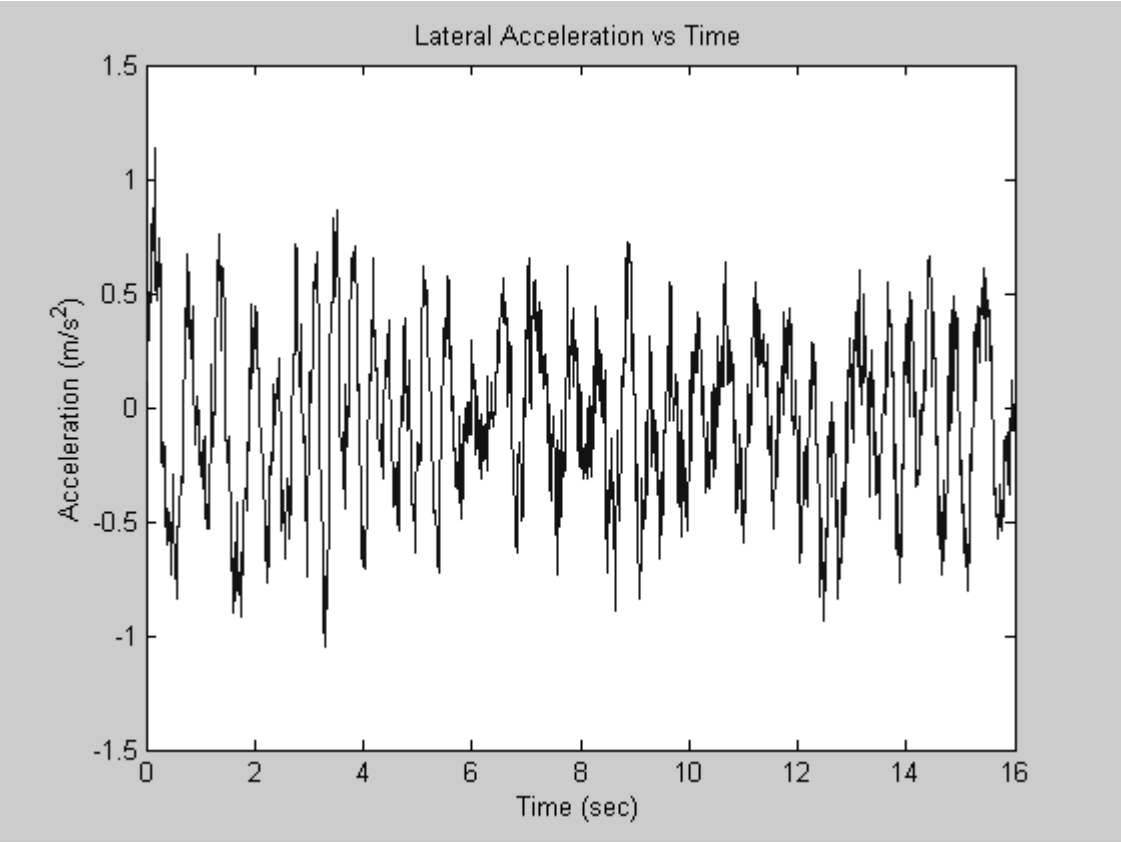

Figure 22: Lateral acceleration of the RC Car during Lane Change

There are many reasons for the discrepancies between the expected and experimental results. The most compelling of these reasons is that the equipment that was used may not have been able to accomplish the task to which they were assigned. Accelerometers are known to be noisy. The accelerometers used in this experiment may not be suitable for this type of research. In the future, the use of a different model of accelerometer or a different type of sensor like a gyroscope should be investigated. Also, Microsoft Windows has been known not to operate well

in the real-time environment, and the interface between Windows and the accelerometers may have resulted in the corruption of the data.

9. Conclusion

During the course of this project, many things were accomplished on the way to the goal of designing a driver assistance steering controller based on the data and testing obtained from a scale model vehicle.

The most important accomplishment was producing a dynamically similar vehicle from the modification of a stock RC car. In doing this, the current RC car can be used in the future to investigate not only the Emergency Turning Maneuver but also many other vehicle situations where the bicycle model applies. In the process of producing the dynamically similar vehicle, several methods were developed to measure and adjust the parameters of the RC car. Of these parameters, the development of the Cornering Stiffness Testing Apparatus and the accompanying procedure was the first of its kind. In the area of control, prototype systems have been designed and tested to control the vehicle's lateral and longitudinal position. With some adjustments, these controllers could be very effective and used in future experimentation. In the area of data acquisition and analysis, procedures have been developed to measure yaw rate and lateral acceleration from accelerometers. While the data gained from these sensors may be flawed, the methods for analyzing the data are correct. The accomplishments of this project place the objective of designing a driver assistance steering controller based on data from tests using scale vehicles within reach.

References

[1] S. N. Brennan, *Modeling and Control Issues Associated with Scaled Vehicles*, Masters Thesis, The University of Illinois, Urbana, IL, 1999.

[2] S. N. Brennan and Andrew Alleyne, "Using a Scale Testbed: Controller Design and Evaluation," *IEEE Control Systems Magazine*, June 2001.

[3] R. W. Allen , H. T. Szostau, and T. J. Rosenthal, "Steady State and Transient Analysis of Ground Vehicle Handling," SAE Paper No. 870498, February 1987.

[4] R. W. Allen, et al., "Vehicle Dynamic Stability and Rollover," Springfield, VA: National Highway Traffic Safety Administration (1992).

[5] J. H. Ginsberg, *Advanced Engineering Dynamics*, New York: Harper and Row Publishers (1988).

[6] R. T. O'Brien, P. A. Iglesias, and T. J. Urban, "Vehicle Lateral Control for Automated Highway Systems," *IEEE Transaction on Vehicular Technology*, vol. 4, no. 3, May 1996.

[7] C.C. Smith, D.Y. McGehee, and A.J. Healey, "The Prediction of Passenger Riding Comfort from Acceleration Data," *Transactions of the ASME, Journal of Dynamic Systems, Measurement, and Control*, vol. 100, March 1978.

Appendix A: Excel Spreadsheet of Vehicle Parameters and Π Groups

	Escort	Civic	Jetta	Le Sabre	S-10
System	english	english	english	english	english
Year	1989	1982	1983	1980	1983
L	7.85	7.58	7.87	9.67	9.81
a	2.96	2.9	2.86	4.28	4.06
b	4.89	4.68	5.01	5.39	5.75
Iz	1135	870	1094.6	3000	2124.01
m	84	69	66.21	125	91.545
Pi(1)	0.377070064	0.382586	0.363405	0.442606	0.413863
Pi(2)	0.622929936	0.617414	0.636595	0.557394	0.586137
Pi(5)	0.219269013	0.219448	0.266921	0.25666	0.241093

	Ranger	F-150	Blazer	Wrangler
System	english	english	english	english
Year	1988	1987	1983	1989
L	9.51	11.12	8.37	7.81
a	4	4.52	3.88	3.63
b	5.5	6.6	4.49	4.17
Iz	1995.006	3980.258	2100	1381.315
m	92.322	142.68	122.5	98.539
Pi(1)	0.420609884	0.406475	0.46356	0.464789
Pi(2)	0.578338591	0.593525	0.53644	0.533931
Pi(5)	0.238934008	0.2256	0.244699	0.229817

Appendix B: Cornering Stiffness and Corresponding Π Groups

Actual Automobiles

Model	Escort	LeSabre	Ranger	Wrangler
Year	89	80	88	89
Kmu	0.234	0.234	0.234	0.234
A0	0	5000	2430	7780
A1	15.66	6.4	9.51	4.56
A2	2350	3700	4040	3680
Weight/2	1275	1915	1485	1585
Percent	0.6235	0.5574	0.5791	0.5347
Fz (lbs)	794.9625	1067.421	859.9635	847.4995
Fz (N)	3536.168	4748.123	3825.307	3769.864
Ca (eng)	4955.997	5932.336	5334.78	6470.135
m (slug)	84	125	92.3	98.54
L (ft)	7.85	9.67	9.51	7.81
U (mph)	17	17	17	17
U (ft/s)	24.93334	24.93334	24.93334	24.93334
Pi 3	0.745007	0.738212	0.884167	0.82488

RC Car Tires

Tire model	OEM	HPI	STS	Purple	Pink
Ca (metric)	42.73	50.4	38.7	25.8	30.2
m (kg)	2.1183	2.1183	2.1183	2.1183	2.1183
L (m)	0.259	0.259	0.259	0.259	0.259
U (m/s)	1.97	1.97	1.97	1.97	1.97
Pi 3	1.34621	1.587853	1.219245	0.81283	0.951452

Appendix C: Longitudinal Control System

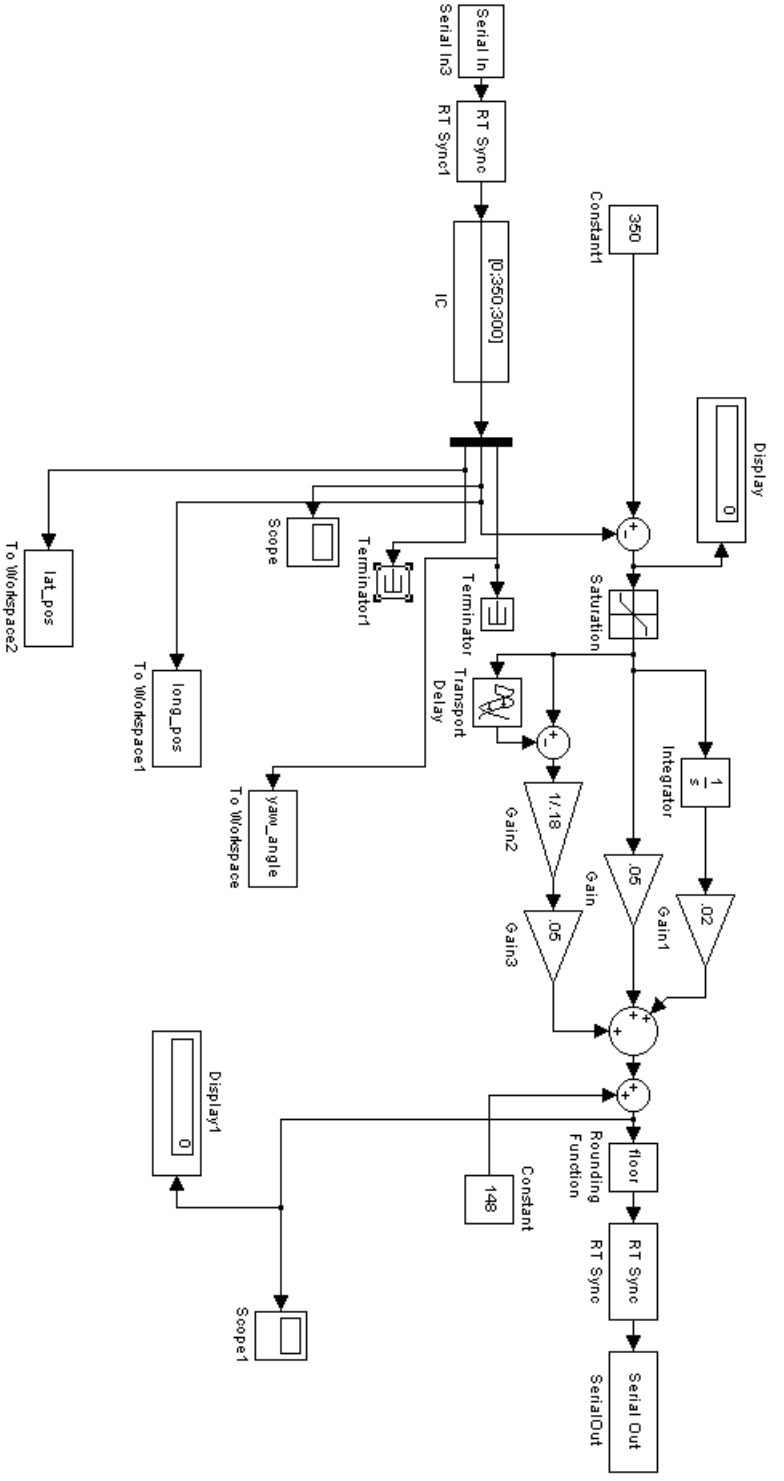

Appendix D: Lateral and Longitudinal Control System